





3 1293 01691 9023

This is to certify that the  
thesis entitled  
**DESIGN OF INITIATING SYSTEMS FOR ULTRAVIOLET  
PHOTOPOLYMERIZATION OF THICK POLYMER  
AND COMPOSITE PARTS**

presented by

**Vijaykumar Narayanan**

has been accepted towards fulfillment  
of the requirements for

M.S. degree in Chem Engineering

Major professor

Date Oct. 6, 1997

**LIBRARY**  
**Michigan State**  
**University**

**PLACE IN RETURN BOX**  
to remove this checkout from your record.  
**TO AVOID FINES** return on or before date due.

DATE DUE	DATE DUE	DATE DUE
11 4 14		

**DESIGN OF INITIATING SYSTEMS FOR ULTRAVIOLET  
PHOTOPOLYMERIZATION OF THICK POLYMER AND COMPOSITE PARTS**

**By**

**Vijaykumar Narayanan**

**A THESIS**

**Submitted to  
Michigan State University  
in partial fulfillment of the requirements  
for the degree of**

**MASTER OF SCIENCE**

**Department of Chemical Engineering**

**1997**

## ABSTRACT

### DESIGN OF INITIATING SYSTEMS FOR ULTRAVIOLET PHOTOPOLYMERIZATION OF THICK POLYMER AND COMPOSITE PARTS

By

Vijaykumar Narayanan

Photopolymerization offers many advantages that could be exploited for polymer composites processing. In this thesis, several photoinitiator systems were studied to develop criteria for selecting a suitable initiator for the photocuring of thick polymers and composites. To aid in this choice, a mathematical model was developed to describe the photobleaching of photoinitiators dissolved in non-reactive solvents. This model is based upon the set of coupled partial differential equations describing the spatial and temporal evolution of the light intensity gradient. The model was verified experimentally for four different  $\alpha$ -cleavable photoinitiators. A procedure was developed to evaluate the suitability of several photoinitiators for UV curing of thick polymer and composite parts based upon their absorption spectra, emission spectrum of the UV light source, transmittance of the resin and cure time of thick polymer samples. Bis(2,4,6-trimethylbenzoyl)phenyl phosphine oxide (BAPO) at a concentration of 0.2 wt % was found to be the most suitable for UV curing of thick vinyl ester samples. Finally, the mechanical properties of the UV cured composite specimens was found to be comparable to specimens cured by conventional methods.

## ACKNOWLEDGEMENTS

Foremost, I would like to thank my advisor Dr. Scranton for his guidance, support and encouragement throughout the course of my graduate studies. I will always look to him for advice in the future too.

I would like to thank Khanh and Rick, for contributing to this work by carrying out several experiments. Their work is greatly appreciated.

I would like to express my appreciation to Julie and Shail, for acquainting me with the lab and for their advice on several matters both technical and non-technical.

I would like to thank Arvind, Bernie, Bharath, Katy and Kiran for making my experience in the research group interesting and enjoyable.

Finally, I would like to thank my parents for their support and encouragement to pursue graduate studies.

## TABLE OF CONTENTS

### CHAPTER 1

#### INTRODUCTION

1.1 Photopolymerizations.....	1
1.2 Photopolymerization: Advantages and Application.....	1
1.3 Photopolymerization of Composites .....	2
1.4 List of References.....	4

### CHAPTER 2

#### BACKGROUND

2.1 Issues associated with photopolymerization of composites .....	5
2.2 Photocured dental composites .....	6
2.3 Industrial Composites.....	8
2.4 Initiators for Photopolymerization of Composites .....	13
2.5 List of References.....	18

### CHAPTER 3

RESEARCH OBJECTIVES .....	20
---------------------------	----

### CHAPTER 4

#### MATHEMATICAL MODEL FOR PHOTOINITIATION OF THICK POLYMERS PARTS: MONOCHROMATIC PHOTBLEACHING IN SOLUTION

4.1 Introduction .....	21
4.2 Description of the System Being Modeled.....	23
4.3 Materials and Method.....	24
4.4 Development of the Model .....	25
4.5 Results and Discussion.....	27
4.6 Effect of Diffusion.....	29
4.7 Conclusions .....	32
4.8 List of References.....	44
4.9 List of Symbols.....	45
4.10 Appendix .....	46

**CHAPTER 5**  
**INVESTIGATION OF PHOTOINITIATING SYSTEMS FOR**  
**PHOTOPOLYMERIZATION OF COMPOSITES**

5.1 Introduction .....	55
5.2 Experimental .....	57
5.3 Results and Discussion.....	60
5.4 Conclusions .....	68
5.5 List of References.....	81

**CHAPTER 6**  
**SUMMARY AND RECOMMENDATIONS**

6.1 Summary .....	82
6.2 Recommendations for Future Work.....	83
6.3 List of References.....	85

## LIST OF TABLES

### *Chapter 4*

<b>Table 4.1</b>	Comparison of theoretical and best fit values of $\gamma$ for different photoinitiators.....	38
------------------	--	----

### *Chapter 5*

<b>Table 5.1</b>	Optimum concentration and cure times for three different photoinitiators for curing 0.9 cm thick sample of Derakane 510A with a light intensity of 65 mW/cm <sup>2</sup> UVA.....	67
<b>Table 5.2</b>	Effect of sample thickness on optimum concentration of BAPO.....	69

## LIST OF FIGURES

### *Chapter 2*

- Figure 2.1 Molecular structure of Benzoin ethyl ether (BEE), a representative  $\alpha$ -cleavage photoinitiator ..... 16
- Figure 2.2 Absorption spectrum of BEE showing the  $\pi \rightarrow \pi^*$  and  $n \rightarrow \pi^*$  absorption bands..... 16
- Figure 2.3 Photochemistry of BEE in solution ..... 17

### *Chapter 4*

- Figure 4.1 Time evolution of the absorbance spectrum of a bis-acyl phosphine oxide (BAPO) photoinitiator as it is irradiated with low intensity UV light. The 2.5 cm thick sample containing  $5.1 \times 10^{-4} \text{ g ml}^{-1}$  of the initiator dissolved in acetone was illuminated from above with filtered light from a mercury lamp. The light was passed through a 10 nm bandpass filter centered at 360 nm, and the intensity at the top surface of the sample was  $2 \text{ mW cm}^{-2}$  ..... 34
- Figure 4.2 Elimination of the intensity gradient in a 1cm thick solution of BEE. The concentration of BEE is  $5 \times 10^{-4} \text{ g/ml}$  and the incident light intensity is  $5 \text{ mW/cm}^2$  at 330 nm..... 35
- Figure 4.3 Elimination of the light intensity gradient in a 1cm thick solution of TPO. The concentration of TPO is  $5 \times 10^{-4} \text{ g/ml}$  and the incident light intensity is  $5 \text{ mW/cm}^2$  at 360nm ..... 35
- Figure 4.4 Change in transmittance as a function of time for a 1cm thick solution of TPO irradiated with 360nm light of intensity  $5 \text{ mW/cm}^2$  ..... 36
- Figure 4.5 Change in transmittance as a function of time for a 3cm thick solution of TPO irradiated with 360nm light of intensity  $5 \text{ mW}$ ..... 36

Figure 4.6	Change in transmittance as a function of time for a 5cm thick solution of TPO irradiated with 360 nm light of intensity 5 mW/ cm <sup>2</sup> .....	37
Figure 4.7	Effect of solvent absorbance on the evolution of the transmittance of a 3cm thick solution of TPO in a solvent with an extinction coefficient of 0.5 ml/gm.cm and 0.8 gm/ml density. The concentration of TPO is 5 x 10 <sup>-4</sup> g/ml and intensity of the incident light is 5 mW/cm <sup>2</sup> .....	37
Figure 4.8	Comparison of theory and experiment for photobleaching of TPO .....	38
Figure 4.9	Comparison of theory and experiment for the photobleaching of TPO .....	39
Figure 4.10	Comparison of theory and experiment for the photobleaching of TPO .....	39
Figure 4.11	Comparison of theory and experiment for the photobleaching of BAPO ....	40
Figure 4.12	Comparison of theory and experiment for the photobleaching of BAPO ....	40
Figure 4.13	Comparison of theory and experiment for the photobleaching of BEE .....	41
Figure 4.14	Comparison of theory and experiment for photobleaching of substituted titanocene.....	41
Figure 4.15	Effect of diffusion on the photobleaching rate of BEE. The concentration is 10 <sup>-3</sup> g/ml and the light intensity is 2.8 mW/cm <sup>2</sup> @ 330nm.....	42
Figure 4.16	Effect of diffusion on the photobleaching rate of BEE. The concentration is 10 <sup>-3</sup> g/ml and the light intensity is 10 mW/cm <sup>2</sup> @ 330nm.....	42
Figure 4.17	Effect of diffusion on the photobleaching rate of BEE. The concentration is 3.3 x 10 <sup>-3</sup> g/ml and the light intensity is 10 mW/cm <sup>2</sup> @ 330nm.....	43

Figure 4.18	Effect of diffusion on the photobleaching rate of BEE. The concentration is $2.79 \times 10^{-4}$ g/ml and the light intensity is $0.8 \text{ mW/cm}^2$ @ 330nm .....	43
Figure 4.19	Comparison of experimental and model data (with and without diffusion) for the photobleaching of BEE .....	44
Figure 4.20	Effect of initiator diffusion coefficient on the photobleaching process. The light intensity is $10 \text{ mW/cm}^2$ and the concentration is $3.3 \times 10^{-3}$ g/ml. All the intensity gradients shown are at time = 900 seconds.....	44
Figure 4.21	Comparison of the photobleaching rate of BAPO and BEE. Both the solutions had the same initial absorbance of 1 and solution depth of 2 cm. The light intensity used for bleaching was $2.2 \text{ mW/cm}^2$ .....	45

### *Chapter 5*

Figure 5.1	Variation of temperature as a function of time at the bottom of thick samples which are photopolymerized under adiabatic conditions .....	74
Figure 5.2	Transmittance spectrum of Derakane 510A in the 300-500 nm range. The path length used was 1 cm .....	74
Figure 5.3	Plot of the extinction coefficient of Derakane 510A as a function of wavelength in the 350-550 nm range. The density of the resin is 1.2 gm/ml. ....	75
Figure 5.4	Comparison of the transmittance spectra of three different resins in the 300-550 nm range. The path length used was 1 cm in all cases.....	75
Figure 5.5	Emission Spectrum of the 1000 W Hg vapor lamp in the 280-500 nm region.....	76
Figure 5.6	Emission spectrum of 1000 W Hg vapor lamp in the 280-500 nm region after it is transmitted through 0.9cm thick layer of Derakane 510A resin. ...	76

Figure 5.7	Absorption spectrum of Benzoin Ethyl Ether. The concentration is $5.1 \times 10^{-4}$ g/ml in acetone .....	77
Figure 5.8	Absorption spectrum of TPO. The concentration is $6.4 \times 10^{-4}$ g/ml in 2-propanol.....	77
Figure 5.9	Absorption spectrum of BAPO. The concentration is $5.1 \times 10^{-4}$ g/ml in acetone.....	78
Figure 5.10	Optimum concentration of TPO for curing 0.9 cm thick sample of Derakane 510A. The light intensity used was $65 \text{ mW/cm}^2$ UVA.....	78
Figure 5.11	Optimum concentration of BAPO for curing 0.9 cm thick sample of Derakane 510A. The light intensity used was $65 \text{ mW/cm}^2$ UVA. ....	79
Figure 5.12	Optimum concentration of BEE for curing 0.9 cm thick sample of Derakane 510A. The light intensity used was $65 \text{ mW/cm}^2$ UVA. ....	79
Figure 5.13	Radicals formed by photolysis of TPO.....	80
Figure 5.14	Radicals formed during complete photolysis of BAPO .....	81
Figure 5.15	Comparison of the absorption spectra of TPO and BAPO in the 320-450 nm spectral region .....	82
Figure 5.16	Maximum temperature measured by the thermocouple during BAPO initiated photopolymerizations of 0.9 cm thick samples of Derakane 510A. The light intensity used was $65 \text{ mW/cm}^2$ UVA .....	82
Figure 5.17	Maximum temperature measured by the thermocouple during TPO initiated photopolymerizations of 0.9 cm thick samples of Derakane 510A. The light intensity used was $65 \text{ mW/cm}^2$ UVA .....	83

Figure 5.18	Effect of light intensity on cure time of 0.9 cm thick sample of Derakane 510A .....	83
Figure 5.19	Comparison of emission spectra of Hg vapor lamp after passing through 0.9 cm thick sample of Derakane 510A resin with and without BAPO photoinitiator .....	84
Figure 5.20	Absorbance spectrum of Bis [ $\eta^5$ -2,4-Cyclopentadien-1-yl] bis[2,6-difluoro-3-[1H-Pyrrol-1-yl] phenyl titanium. The concentration is $2.4 \times 10^{-3}$ g/ml in acetone .....	84
Figure 5.21	Absorption spectrum of Camphorquinone in the 380-520 nm region. The concentration is $5.01 \times 10^{-3}$ g/ml in acetone .....	85
Figure 5.22	Comparison of flexural strength of composites. The bar represents the average value (of 5 samples) while the error bars represent the high and low values obtained in the tests.....	85

# Chapter 1

## Introduction

### 1.1 Photopolymerization

Photopolymerization is generally a chain polymerization in which the propagating active centers (usually radicals or cations) are produced by a photochemical event. A wide variety of chemical compounds (photoinitiators) are available that produce free radicals upon absorption of photons of the appropriate energy (typically in the UV or visible region of the spectrum). The photochemical mechanism of active center generation has been well characterized, and generally proceeds by  $\alpha$ -cleavage,  $\beta$ -cleavage or hydrogen abstraction<sup>1,2</sup>.

### 1.2. Photopolymerization: Advantages and Applications

Light-induced polymerizations offer many advantages that may be exploited in industrial processes. For example, photopolymerizable formulations are typically solvent-free, which is important for coating applications because volatile organic emissions are a major concern. As active centers may be produced rapidly and efficiently using photochemical processes, Photopolymerization offers high production rates and is very energy efficient compared to thermal systems in which the entire reaction system is raised to elevated temperatures. Finally, photopolymerizations provide a great deal of control over the initiation reaction: spatial control, because the light may be directed to locations of interest in the system; and temporal control, because the light may be readily

shuttered on or off.

The advantages afforded by photopolymerization have led to tremendous growth in applications of these reactions. Light-induced polymerizations are now widely used for films, inks and coatings on a variety of substrates including paper, metal, plastic and wood; dental materials for which the initiating light is routed into the mouth using optical fibers; and a variety of high-tech and electronic applications such as coatings on optical fibers, replication of optical disks, and fabrication of printed circuit boards. Finally, a relatively recent application of radiation curing is in the area of stereolithography for the production of three-dimensional prototypes using data generated by a computer aided design (CAD) software package.

### **1.3. Photopolymerization of Composites**

While the traditional thin-film applications of photopolymerization are experiencing rapid growth in their own right, the advantages afforded by these reactions also make them attractive for the development of new processes for producing fiber-filled polymer composites. Most notably, the spatial and temporal control of initiation offered by photopolymerizations provides 'cure on demand', which could be used to achieve short cycle times while circumventing many problems and limitations of current composites production methods. Composites for the durable goods industry are typically produced by resin transfer molding (RTM) or filament winding processes in which a free radical polymerization is triggered using thermal initiators. In these thermally initiated processes, the time required for heat transfer places a lower limit on the cycle time, and

attempts to reduce the cycle time by preheating the mold (in RTM) or the resin (in filament winding) invariably lead to problems associated with premature cure, or very complicated flow patterns. Finally, the energy efficiency and low capital cost associated with UV curing may provide additional benefits. Photopolymerization may offer enhanced energy efficiency because it generally is performed at room temperature without external heating. In addition, the light sources used in photopolymerization may be considerably less expensive than the large autoclaves used for thermal polymerizations.

As an example of how the cure on demand afforded by photopolymerizations could lead to improvements in composites manufacturing, it is useful to consider the RTM process. In this method, a reacting resin is injected into a closed mold containing the fiber preform. Short cycle times necessitate a careful balance between the conflicting requirements of rapid mold filling and high polymerization rates. This trade-off leads to a very complicated flow process in which a reacting liquid is forced through a porous medium (the preform). As the liquid reacts it becomes more viscous (actually viscoelastic), leading to several important problems associated with high operating pressures, poor resin impregnation into the fibers, preform displacement, and gelation of the resin in the transfer lines. These problems, which ultimately arise from the fact that the mold-filling and reaction are coupled to one another, are exacerbated by attempts to reduce the cycle time by using more reactive resins.

The temporal control offered by photopolymerizations could be exploited to alleviate many of the problems associated with RTM by: (1) allowing the mold to be completely filled with a low-viscosity resin before any reactions takes place, and (2)

initiating a fast thermoset reaction after the mold is completely filled<sup>3</sup>. This decoupling of mold filling and reaction would permit complete control of the time allowed for micro-flow, and would reduce waste and expensive clean-up by preventing premature reaction (gelation in the transfer lines). In addition, unlike traditional processes, the photoinitiated reactions are not limited by the rate of heat transfer from the mold to the resin, and would consequently offer short cycle time. Finally, since there would be no need for high pressures or external heating of the die, the proposed process would be very energy efficient. Other composite processing methods such as filament winding would benefit in a similar manner from the cure on demand afforded by photopolymerizations.

#### **1.4 List of References**

1. J.P. Fouassier, *Photoinitiation Photopolymerization and Photocuring Fundamentals and Applications*, Hanser Publishers, 1995
2. J.P. Fouassier in *Radiation Curing in Polymer Science and Technology* (Vol. 2) (Fouassier, J. P., and Rabek, J.F., eds), pp.1-61, Elsevier Applied Science, 1993
3. L.S. Coons, B. Rangarajan, D. Godshall, A.B. Scranton In *Innovative Processing and Characterization of Composite Materials* (Vol. 20) (Gibson, R.T., Chou, T.W., Raju, P.K., eds.), pp.227-240, ASME, New York, 1995

## **Chapter 2**

### **Background**

#### **2.1. Issues associated with photopolymerization of composites**

Photopolymerizations of thick and fiber-filled polymers are more challenging than polymerizations of thin-film systems due to the exponential reduction in light intensity through the sample resulting from absorption and scattering. For this reason, issues that are relatively unimportant for thin-film photopolymerizations can make the difference between success and failure for thick and fiber-filled systems. For example, an initiator concentration that is too high, or even a small resin extinction coefficient at the initiating wavelength can prevent efficient cure throughout the sample. Therefore, for thick polymers and composites, proper selection of the initiator formulation and illumination wavelength are imperative to ensure that the samples cure throughout (including the portions of the sample furthest from the light).

For photopolymerization of composites for the durable goods industry, light from the near UV region of the spectrum between 330 and 420 nm is the most convenient initiating source. This arises as a result of several factors. First, visible light is usually avoided to prevent premature cure triggered by ambient light. In addition, deep UV light is inappropriate due to absorbance by the resin and/or fibers. Finally, there are several commercially available initiators that absorb in this region, and inexpensive mercury lamps have prominent emissions in this spectral region.

As mentioned previously, careful selection of the illumination source, initiator

system (type of initiator, photosensitizer, concentration etc.), resin, fiber reinforcement and composite thickness are imperative for successful photopolymerization of composites. Thus the cure behavior of the composite is dependent upon several different variables, which must be carefully controlled. Similar problems have been encountered in other applications such as photocurable dental restoratives. Hence, it is useful to briefly examine the literature in this area to obtain some insight into the strategies that could be used for photopolymerization of composites.

## **2.2 Photocured dental composites**

Photopolymerization has been used in dental applications since 1970, when UV-cured fissure sealants were reported using benzoin methyl ether as the photoinitiator<sup>1</sup>. In the past few decades, photopolymerization has become prominent for curing dental materials, and only representative references related primarily to depth of cure issues will be discussed here. Some applications and issues associated with photopolymerization of dental materials are described in recent reviews<sup>2,3</sup>. Most photocured dental materials consist of a multifunctional acrylate or methacrylate resin, an initiator and a powdered glass reinforcement with particle size between 0.7 and 50  $\mu\text{m}$ . Today, dental composites are cured using visible (blue) light due to safety considerations and ease of handling.

The depth of cure is an important aspect of photocured dental composites and numerous investigators have studied this issue. For example, Kilian<sup>2</sup>, Cook<sup>4</sup>, Salako and Cruickshanks-Boyd<sup>5</sup> and Tirtha *et al.*<sup>6</sup> characterized the hardness of photocured dental composites as a function of sample depth (several millimeters) and have concluded that

the hardness decreases considerably from top to bottom (due to the variation of light intensity with sample depth). Cook<sup>4</sup> conducted a theoretical study of the variation of cure time with sample thickness and predicted a logarithmic relation between cure depth and time, in agreement with his experimental results. This model was based upon the assumption of a static light intensity gradient, and included the effects of an inhibitor that prevents polymerization below a threshold active center concentration.

Kawaguchi *et al.*<sup>7</sup> characterized the relationship between cure depth and transmission coefficient of visible-light-initiated dental composites up to seven millimeters thick and fitted the results to a linear correlation. These authors also investigated the effect of particle size on the depth of cure and found that microfilled resins with particle size of 0.04  $\mu\text{m}$  exhibited a lower cure depth than resins filled with particles of size ranging from 0.2 to 50  $\mu\text{m}$ . This effect was attributed to enhanced scattering by the smaller particles. Leung *et al.*<sup>8</sup> studied the post-irradiation cure of dental composites and reported a continuous increase in hardness that plateaued after about a day, which they attributed to dark-cure. Similarly, Kolarik *et al.*<sup>9</sup> found a perceptible increase in glass transition temperature and flexural modulus of the composite after storage in the dark. In addition, both Kolarik *et al.*<sup>9</sup> and Taira *et al.*<sup>10</sup> reported that elevating the temperature of the illuminated sample resulted in significant post-cure (as evidenced by enhanced thermal and mechanical properties), which they attributed to the presence of residual living radicals. Finally, Maffezzoli *et al.*<sup>11</sup> reported that the degree of cure of the dental resins under nonisothermal conditions (when the heat of polymerization is not immediately removed, thereby causing the temperature to increase)

was considerably higher than the degree of cure under controlled isothermal conditions.

This review of the dental composites literature provides some important information that can be exploited for photopolymerization of fiber glass composites for the durable goods industry. Foremost, the work on dental composites has demonstrated that photopolymerization can be used to cure relatively thick samples (not just thin films), and has provided guidelines for the design of these reaction systems. Indeed, in some ways the photopolymerization of industrial composites are easier than their dental counterparts because fewer constraints are placed on the initiation wavelengths, reaction temperature etc. For example, the industrial composites could be cured with UV rather than visible light, and a higher temperature may be tolerated (burning the patient is a concern for dental composites) and can be exploited to obtain higher conversions at shorter cycle times.

### **2.3 Industrial composites**

While there are literally hundreds of papers covering photopolymerization of dental composites, there are relatively few articles on photopolymerization of composites for industrial (durable goods) applications. The discussion of this area will be organized in two sections. It will begin with a survey of laboratory studies of photopolymerization in thick and fiber-filled systems to illustrate the trends and operating principles that have been identified by several research groups. Next a few commercial applications of composites photopolymerization that have been reported to date will be discussed.

*Laboratory studies of composite photopolymerizations*

In a series of papers, Ogale and co-workers<sup>12-15</sup> examined photopolymerization of acrylate - glass fiber systems for three-dimensional stereolithography applications. These investigators examined a variety of glass reinforcements, including continuous and chopped glass fibers, as well as 55  $\mu\text{m}$  diameter borosilicate glass spheres. Based upon measurements of the mechanical properties of the resulting composites, these authors concluded that photolithography of composites is indeed feasible<sup>12,13</sup>. These investigators also used dynamic mechanical analysis to examine the effects of glass, quartz and carbon fibers on the photopolymerization rate of acrylate composites<sup>14</sup>. The authors reported that the glass and quartz fibers had essentially no effect on the cure rate, while the carbon fibers reduced the rate of photopolymerization due to absorption of light.

Shi and Ranby<sup>16</sup> reported photopolymerizations of glass-fiber-polyester composites. These authors used unsaturated polyester resins that were end-capped with acrylate groups, and included multifunctional acrylic, allylic or acrylether comonomers as reactive diluents. Chopped e-glass fiber mats were used for the composite reinforcement, and laminates that were approximately 2 mm thick (containing four or five layers of the glass fiber mats) were prepared. The investigators found that the laminates could be cured rapidly upon illumination with a high-pressure mercury lamp, and that the resulting composites exhibited excellent mechanical properties. In addition, they found that the acrylate or acrylether reactive diluents enhanced the mechanical properties more than the allylic comonomers. They attributed this trend to fact that the allylic comonomers

undergo hydrogen abstraction reactions with the initiator radicals<sup>16</sup>. Shi and Ranby<sup>17</sup> also prepared glass-reinforced composites using dendritic methacrylated polyesters as the matrix. They found that photopolymerization allowed the composites to be cured more rapidly than thermal polymerization with no deleterious effects on the mechanical properties. The authors concluded that the dendritic polyesters are promising for industrial glass-fiber-reinforced composites.

Coons *et al.*<sup>18</sup> investigated photopolymerizations of thick polymers and glass-fiber-filled composites using commercially available vinyl ester resins and inexpensive benzoin ether initiators. These investigators have examined two strategies for efficient photopolymerization of thick polymers samples and composites using UV light as the sole (external) initiating source. The first method involves careful selection of the initiating wavelength (such that the resin and fibers are transparent to the initiating wavelength) and use of photobleaching initiators to ensure penetration of light into the sample. Photobleaching occurs when the products of photolysis exhibit less absorbance than the photoinitiator at the wavelength of interest<sup>1,19</sup>. For example, the efficient photobleaching of the initiator bis(2,4,6-trimethylbenzoyl) phenyl phosphine oxide is illustrated in Figure 4.1 (Chapter 4). The figure illustrates that the broad absorption peak between about 360 and 400 nm decreases dramatically in intensity as the illumination time is increased, thereby allowing the light to penetrate more deeply into the sample. Coons *et al.*<sup>18</sup> characterized the effects of process variables such as light intensity, cure time, initiator concentration and fiber loading on the mechanical properties of the final composite. In agreement with previous results for unfilled systems<sup>20</sup>, an optimum

initiator concentration was observed above which or below which the photopolymerization was less efficient.

The second composite polymerization strategy investigated by Coons *et al.*<sup>18</sup> was a dual-cure strategy in which both a photoinitiator and a thermal initiator are included in the reaction mixture. Here, the heat evolved from an exothermic photopolymerization elevates the temperature and results in the production of additional active centers by the thermal initiator. In experiments performed using standard vinyl ester resins, measurement of temperature profiles *in situ* revealed that the reaction exotherm is high enough to ensure adequate polymerization and property development without leading to thermal degradation. These results suggest that the dual cure strategy offers both the temporal control of the start of the reaction afforded by the photopolymerization, as well as the enhanced reaction rate and completeness of cure provided by the thermal initiation.

Medenouvo and Fouassier<sup>21</sup> investigated photopolymerizations of unsaturated polyester - styrene resins filled with glass fibers. In agreement with the studies discussed above, the authors found that the mechanical properties of the photocured composites were similar to those produced using conventional methods. One objective of their study was to identify an initiator system that makes optimum use of the light emitted from a number of light sources; therefore they experimented with a variety of photoinitiators, photosensitizers, thermal initiators and additives. Based on their experiments they reported an optimum formulation containing 0.15 wt% phenonyl oxime ester (the photoinitiator), 0.02 wt% eosin (a photosensitizer), 0.02 wt% benzantraquinone (a photosensitizer), 1 wt% methyl diethanolamine (an electron-donating additive), and 0.25

wt% benzoyl peroxide (a thermal initiator) with the remainder of formulation made up of the monomer to be polymerized.

Our final example of laboratory studies on composite photopolymerizations is taken from the patent literature. Bellobono<sup>25</sup> reported organometallic photoinitiators that, when used with organic photosensitizers, are able to efficiently photoinitiate in the near UV (300-400 nm) region. Bellobono used his novel initiator systems to photopolymerize styrenated polyester resins filled with glass or carbon-fibers to produce composites with thicknesses of 1-3 mm. In addition he reported that it is possible to prepare composites as thick as a few centimeters.

#### *Commercial composite photopolymerization systems*

As the manufacture of industrial composites by photopolymerization is in its infancy, few commercial systems have been reported to date. One notable commercial photopolymerization system for fiber-glass composites is a UV-cured vacuum-assisted RTM process<sup>23</sup> developed by Synergistic Composite Systems Inc., using photopolymerizable vinyl ester resins from Sunrez Corporation. The company claims the cure on demand afforded by photopolymerization as an important advantage of their process because mold-filling problems during infusion can be corrected before the UV lamps are turned on<sup>23</sup>. In addition, the resins can withstand temperatures up to 65°C without curing; therefore the resin may be heated to reduce its viscosity<sup>23</sup>, thereby improving mold filling and fiber impregnation. The process was used to cure relatively thick composites in a reasonable period of time. For example, 0.5 in (1.2 cm) thick

laminates were cured in 7-10 minutes<sup>23</sup>. The process was tested for manufacture of a half-scale mid-ship section of a naval combat ship<sup>23</sup>.

A second composite UV-cure process that has been commercialized is the Accuset™ filament winding resin reported by Loctite Corporation<sup>24</sup>. In the Loctite process, a photopolymerization stage (after resin impregnation, before winding) is used to overcome many of the problems and limitations of conventional filament winding processes by producing a viscous, gel state that immobilizes the resin and reduces resin loss. After winding is complete, the cure is completed by a second, thermal stage. The resin formulations typically contain ~14 wt% of a UV-curable acrylate monomer, with the remainder of the formulation made up of a standard, thermally-cured, epoxy-based resin. The company claims that the addition of the UV stage offers many advantages, including faster winding speeds, shorter cure times, instant resin immobilization (which prevents resin dripping), and enhanced control of fiber placement and fiber volume.

#### **2.4. Initiators for Photopolymerization of Composites**

A photoinitiator is the chemical species which produces active centers (free radicals or cations) upon absorption of photons of the appropriate wavelength. In general, free radical photoinitiators fall into two categories: cleavable and non-cleavable photoinitiators. The cleavable photoinitiators directly produce free radicals upon absorption of photons and are further classified according to the mechanism by which they undergo photolysis as  $\alpha$ -cleavable,  $\beta$ -cleavable and  $\gamma$ -cleavable initiators. The non-cleavable initiators require a co-initiator such as an amine (electron transfer agent) or an

alcohol (a hydrogen donor) in order to produce free radicals.

Most of the commonly used free radical photoinitiators fall under the category of  $\alpha$ -cleavable initiators. Such initiators include several families of compounds such as benzoin ethers, dialkoxyacetophenones, hydroxy alkyl ketones, benzoyl phosphine oxides, benzoyl oxime esters, morpholino ketones and amino ketones<sup>25</sup>. Benzoin ethyl ether (Figure 2.1) is a representative  $\alpha$ -cleavable photoinitiator whose photochemical mechanism has been well characterized<sup>26,27,28,29</sup>. Figure 2.2 shows the absorption spectrum of benzoin ethyl ether. It has two distinct absorption bands one in the deep UV region (below 300 nm) and a second smaller band in the UVA region between 300 and 390 nm. Such a spectrum is characteristic of ketone<sup>30</sup>. The more intense absorption band in the deep UV corresponds to a  $\pi \rightarrow \pi^*$  electronic transition. The  $\pi \rightarrow \pi^*$  electronic transition occurs when a  $\pi$  electron of the keto group is promoted to an excited state after absorbing a photon. The smaller band in the near UV region corresponds to a  $n \rightarrow \pi^*$  electronic transition, which occurs when one of the lone pair of electrons on the oxygen of the keto group is promoted to an excited state after absorbing a photon of appropriate wavelength. Figure 2.3 shows the sequence of reactions that occurs when a solution of BEE in benzene is irradiated with light in the UVA region. The BEE upon absorption of a photon is promoted to the excited singlet state. It then undergoes efficient intersystem crossing to the triplet state after which it undergoes photolysis to give rise to two free radicals (a benzoyl radical and an ethoxybenzyl radical). The above steps occur very rapidly and the kinetic constants are as shown in Figure 2.3. In the absence of oxygen,

the free radicals further react and finally form benzaldehyde, benzil and pinacol ethers<sup>27</sup>. In the presence of oxygen, however, the radicals may be captured, resulting in the formation of benzoic acid and esters of benzoic acid<sup>27</sup>. Finally, if unsaturated compounds (such as styrene) are present, then the benzoyl free radicals preferentially add on to the double bonds, thereby initiating a chain polymerization<sup>27</sup>. The kinetic constant for oxygen quenching of the free radicals is about  $10^9 \text{ l mol}^{-1} \text{ sec}^{-1}$ <sup>25</sup> and the kinetic constant for reaction with styrene is about  $10^5 \text{ l mol}^{-1} \text{ sec}^{-1}$ <sup>29</sup>. However, in usual solution photopolymerizations, the concentration of dissolved oxygen is about  $10^{-3} \text{ mol/l}$  and that of the monomer is about  $10^1 \text{ mol/l}$ , so the rate of oxygen quenching and initiation have the same order of magnitude. In bulk polymerizations, however, the concentration of dissolved oxygen is much lower and the concentration of monomer is much higher, hence the oxygen quenching reaction does not compete with the initiation reaction.

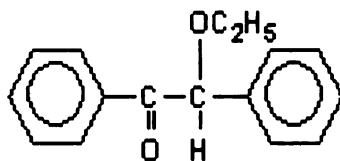


**Figure 2.1.** Molecular structure of Benzoin ethyl ether (BEE), a representative  $\alpha$ -cleavage photoinitiator

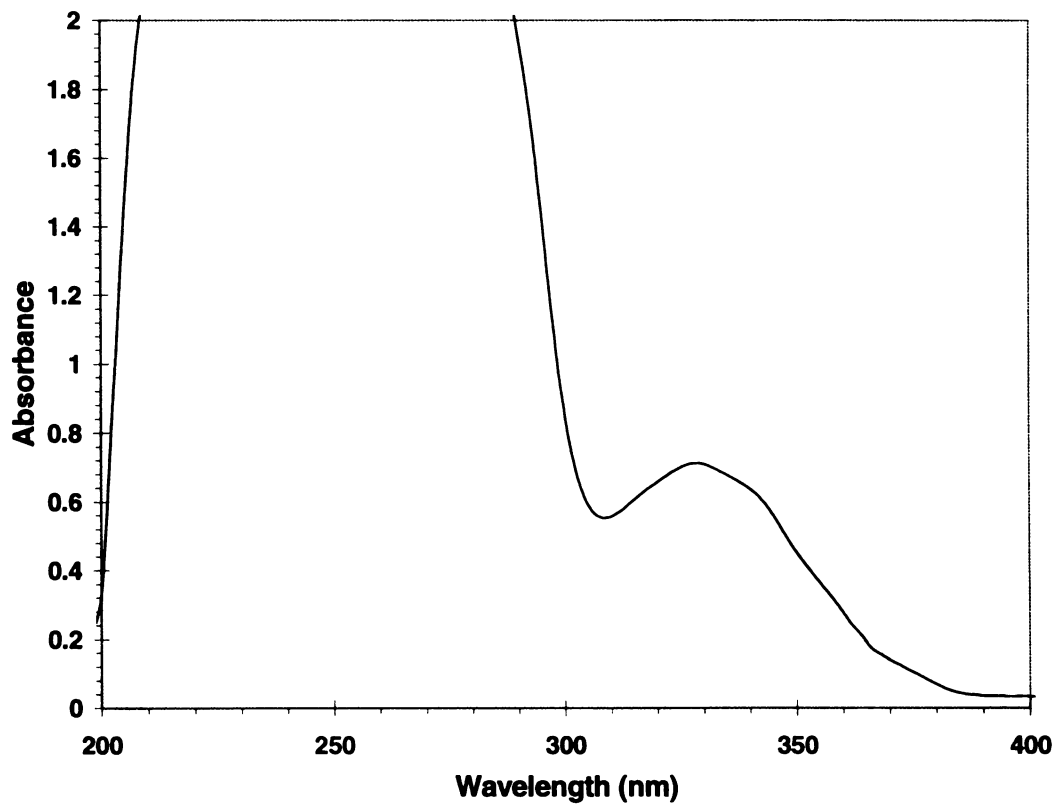


**Figure 2.2.** Absorption spectrum of BEE showing the  $\pi \rightarrow \pi^*$  and  $n \rightarrow \pi^*$  absorption bands

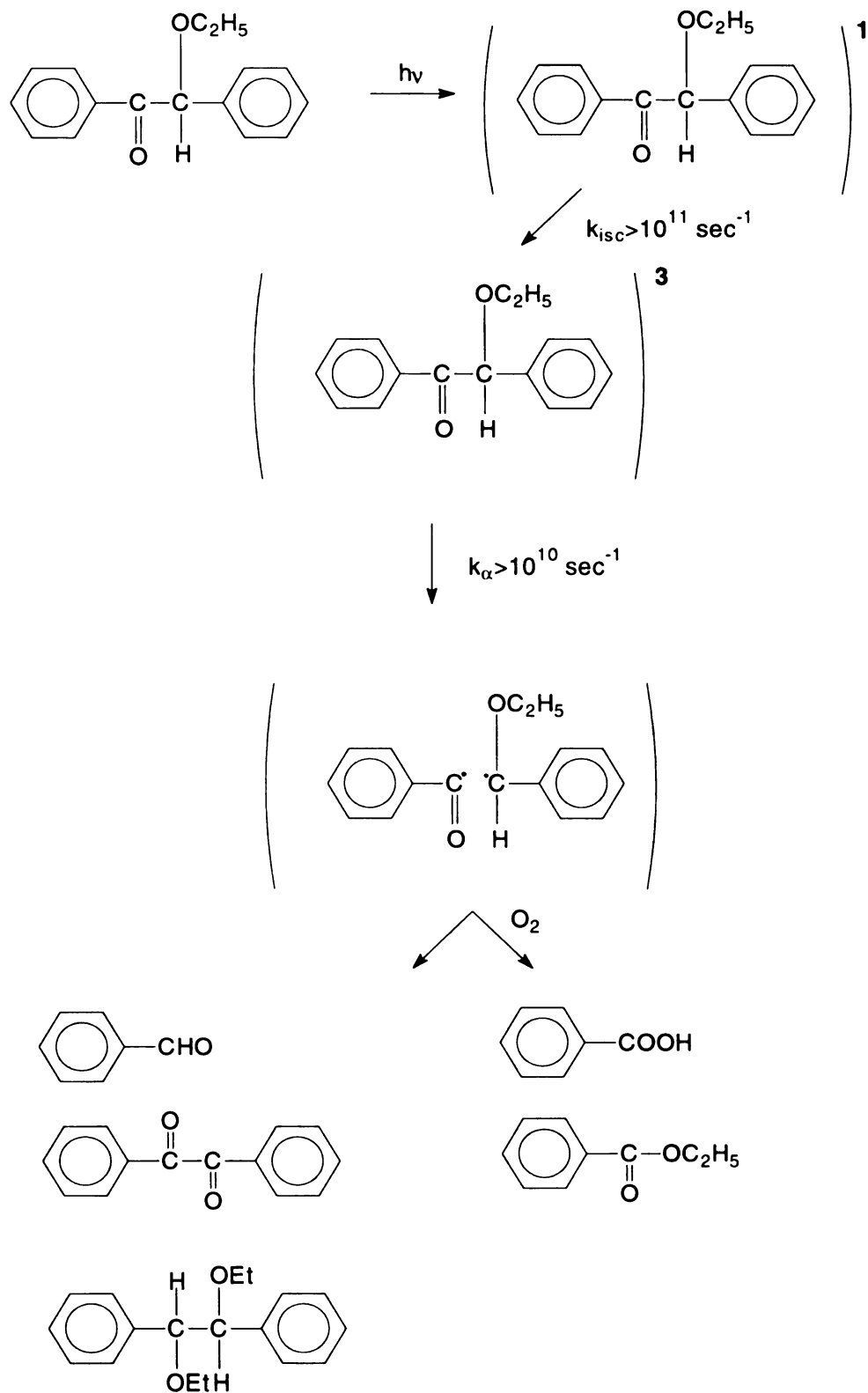


**Figure 2.3.** Photochemistry of BEE in solution

## 2.5. List of References

1. M.G. Buonocore, *J. Am. Dent. Assn.* **80**, 324, 1970
2. R.J. Kilian, in *Polym. Sci. and Tech.* (Vol. 14), Charles G. Gebelein and Frank K. Koblitz, eds, pp. 411-417, Plenum Press, 1980
3. K.S. Anseth, S.M. Newman, C.N. Bowman, in *Advances in Polymer Science* (Vol. 122), Peppas, N.A., Langer, R.S., eds, pp. 177-217, Springer-Verlag, 1994
4. W.D Cook, *J. Dent. Res.* **59**, 800, 1979
5. N.O. Salako, D.W. Cruickshanks-Boyd, *Brit. Dent. J.* **146**, 375, 1979
6. Tirtha, R., Fan, P.L., Dennison., J.B., Powers, J.M., (1982) *J. Dent. Res.* **61**, 1184
7. M. Kawaguchi, T. Fukushima, K. Miyazaki, *J. Dent. Res.* **73**, 516, 1994
8. R.L. Leung, P.L. Fan, W.M. Jonston, *J. Dent. Res.*, **62**, 363, 1983
9. J. Kolarik, C. Migliaresi, P. Capauana, L. Fambri, *Polymers in Medicine*, **4**, 145, 1991
10. M. Taira, A.M. Khan, K. Ohmoto, N. Satou, H. Shintani, K. Wakasa, M. Yamaki, *J. Mat. Sci. Lett.* **13**, 1229, 1994
11. A.M. Maffezzoli, R. Terzi, L. Nicolais, *J. Mat. Sci.:Materials in Medicine* **6**, 161, 1995
12. T. Renault, A.A. Ogale, R.L. Dooley, A. Bagchi, C.C. Jala-Almonte, *SAMPE Quaterly* **22**, 19, 1991
13. T. Renault, A.A. Ogale, R.L. Dooley, A. Bagchi, C.C. Jala-Almonte, *SAMPE Quaterly* **23**, 28, 1991
14. T. Renault, A.A. Ogale, M.J. Drews, *Proc. ANTEC '93*, 2352, 1993
15. T. Renault, A.A. Ogale, *Polym. Eng. Sci.* **36**, 551, 1996
16. Winfang Shi, Bengt Ranby, *J. of App. Polym. Sci.* **51**, 1129, 1994
17. Wenfang Shi, Bengt Ranby *J. Appl. Polym. Sci.* **59**, 1951, 1996

18. L.S. Coons, B. Rangarajan, D. Godshall, and A.B. Scranton, *ACS Symposium Series*, in press
19. J. Finter, M. Riediker, O. Rohde, B. Rotzinger, *Makromol. Chem., Macromol. Symp.* **24**, 177, 1989
20. J. Guthrie, M.B. Jaganathan, M.S. Otterburn, J. Woods, *Polym. Bull.* **15**, 58, 1986
21. F. Medenouvo, J.P. Fouassier, *Angew. Makromol. Chem.* **229**, 29, 1995
22. I.R. Bellobono, European Patent 0 421 512 A1, 1991
23. A. Hudson, *Composites Technol.*, **2**, 24, 1996
24. Y. Okamoto, P. Klemarczyk, S. Levandoski, V. Hanlon, J. Bremmer, *SME Technical Paper EM94-111*, 1, 1994
25. J.P. Fouassier in *Radiation Curing in Polymer Science and Technology* (Vol. 2) (Fouassier, J. P., and Rabek, J.F., eds), pp.1-61, Elsevier Applied Science, 1993
26. F.D. Lewis, R.T. Lauterbach, H.G. Heine, W. Hartmann, H. Rudolph, *J. Am. Chem. Soc.*, **97**, 1519, 1975
27. H.G. Heine, H.J. Rosenkranz, H. Rudolph, *Angew. Chem., Int. Ed. Engl.*, **11**, 974, 1972
28. S. P. Pappas, A. Chattopadhyay, *J. Am. Chem. Soc.*, **95**, 6484, 1973
29. R. Kuhlmann, W. Schnabel, *Angew. Makromol. Chem.*, **70**, 145, 1978
30. J.D. Coyle, *Introduction to Organic Photochemistry*, John Wiley & Sons, 1986

## **Chapter 3**

### **Research Objectives**

From the introduction and background provided, it is clear that photopolymerizations offer tremendous advantages over traditional thermal methods, including low energy requirements, spatial and temporal control of initiation, and high polymerization rates. By careful system design, it is possible to come up with a commercially feasible process for photopolymerization of composites. Indeed, few commercial processes for manufacture of composites for the durable goods industry already exist and there is considerable scope for improvement in technology.

The general objective of this research project is the development of photopolymerization processes for high-speed, low-cost production of polymeric composites. To achieve this general objective, the specific objectives were:

- i. To quantify the photobleaching effect of photoinitiators to aid in making a choice of photoinitiator for curing of thick polymer and composite parts
- ii. To establish a technique for the design of photoinitiating systems for curing of thick polymer and composite parts

To show that UV curing is a viable technology for manufacture of composites

## Chapter 4

### **Mathematical Model for Photoinitiation of Thick Polymers Parts: Monochromatic Photobleaching in Solution**

#### **Abstract**

Many  $\alpha$ -Cleavable photoinitiators exhibit a photobleaching effect in which the absorbance decreases with illumination time when exposed to light of the proper wavelength. For example, benzoin ethers exhibit photobleaching of the absorbance peak between 320 and 365nm. This occurs because the products of photolysis do not absorb in the same region as the original initiator molecule. The net result of the photobleaching is an increase in transmittance of the photoinitiator system as a function of illumination time, as long as the other components of the system (e.g. the monomer) do not absorb significantly in the same wavelength range. The phenomenon of photobleaching is particularly important in the photocuring of thick polymer parts. In this chapter, a mathematical model is developed for the photobleaching effect of photoinitiators dissolved in non-reactive solvents. Given the incident light intensity and wavelength and the initial photoinitiator concentration, the model predicts the variation of the photoinitiator concentration and light intensity with time and sample depth. The model was verified experimentally for four different  $\alpha$ -cleavable photoinitiators

#### 4.1. Introduction

For photopolymerization of thick systems, one of the criteria for choice of photoinitiator is its ability to undergo photobleaching. In general, when a molecule is irradiated with light of a wavelength in which it absorbs, and is promoted to the excited singlet state, it may undergo a number of photophysical processes such as fluorescence, intersystem crossing to the triplet state, phosphorescence, photolysis, hydrogen abstraction, singlet or triplet state quenching *etc*<sup>1</sup>. However, most of the commonly used  $\alpha$ -cleavable free radical photoinitiators undergo a fairly simple sequence of photochemical transitions. They are excited to the singlet state, undergo efficient intersystem crossing to the triplet state and subsequently undergo photolysis to form free radicals. The quantum yield of each of these steps is close to unity. Once formed, the free radicals may further react with one another or with other species in solution (such as oxygen) to produce other products, and if monomer is present, to initiate polymerization.

If the absorption of the photolysis products is less than that of the photoinitiator molecule, then the absorbance of the solution decreases with irradiation time (as shown in Figure 4.1), allowing more light to pass through it. This phenomenon is known as photobleaching<sup>2</sup>. For example, the photolysis products of benzoin ethyl ether (BEE) when irradiated with UV light in a solution of deoxygenated benzene are benzil, benzaldehyde and picanol ethers<sup>3</sup>. These molecules are considerably less absorbing at 365 nm than BEE itself, hence photobleaching is observed upon irradiation of a solution of BEE at 365 nm. Photobleaching is particularly pronounced in solutions of acyl and bisacyl phosphine oxides since photolysis results in cleavage of the carbon phosphorus

bond, thereby destroying the chromophore which absorbs in the in the near UV-Vis region (350-410 nm)<sup>4</sup>. Substituted Titanocenes are another class of photoinitiators which have excellent bleaching properties in the 440 nm region<sup>5</sup>.

Several investigators have emphasized the importance of photobleaching for curing of thick pigmented coatings and thick polymer and composite parts<sup>6,7</sup>. However, little attention has been paid to quantitatively describing this effect. A quantitative description of the photobleaching effect would be particularly useful in comparing the photobleaching effectiveness of different initiators, and thus would provide an important tool for choosing a photoinitiator for applications such as curing of thick polymer and composite parts.

In this contribution, a mathematical model was developed for the photobleaching effect of photoinitiators dissolved in non-reactive solvents. Given the incident light intensity and wavelength and the initial photoinitiator concentration, the model predicts the variation of the photoinitiator concentration and light intensity with time and sample depth. The model equations (a set of coupled partial differential equations) were solved using software packages (Mathcad and Excel) and the simulation predictions were compared to experimental results.

#### **4.2. Description of the System Being Modeled**

A mathematical model was developed to describe the spatial and temporal evolution of the light intensity gradient in thick photobleaching systems. The system being modeled consists of a dilute solution of a photoinitiator (of known depth) which is

illuminated with monochromatic light from above. Both the photoinitiator and the solvent may absorb at the wavelength under consideration, therefore the light intensity changes with sample depth. However since the photoinitiator undergoes photobleaching, the intensity gradient in the sample changes with depletion of photoinitiator. In fact at any point below the sample surface, the intensity increases with time. Thus the light intensity and photoinitiator concentration in the sample are functions of both time and sample depth. The model predicts the variation of light intensity and concentration with sample depth and time, given the incident light intensity, wavelength and the initial photoinitiator concentration.

### 4.3. Materials and Method

#### *Materials*

The photoinitiators chosen for this study were benzoin ethyl ether (BEE, Aldrich), 2,4,6-trimethyldiphenylbenzoylphosphine oxide (TPO, Aldrich), 2,4,6-bis(trimethylbenzoyl) phenylphosphine oxide (BAPO, Ciba-Geigy), and bis[ $\eta^5$ -2,4-Cyclopentadien-1-yl] bis[2,6-difluoro-3-[1H-pyrrol-1-yl]phenyl] titanium (a substituted titanocene, Ciba-Giegy). The solvents used were acetone (J.T. Baker), 2-propanol (J.T. Baker) and methyl ethyl ketone (Mallinckrodt). The substituted titanocene received from Ciba-Giegy actually contains a blend of the pure photoinitiator and an inert clay. The mixture was dissolved in methyl ethyl ketone and centrifuged at 2000 rpm for about 10 minutes, in order to precipitate out the inert clay. The other chemicals were used as received.

### *Experimental Procedure*

The photoinitiator solution was exposed to light from a 1000 W mercury-xenon lamp (Oriel Corp.). A water filter was used to remove the IR radiation emitted by the lamp, and interference filters were used to select the desired illumination wavelength. The light intensity at the sample surface was measured using a Scientech 362 energy meter. A photoinitiator solution of known depth was placed in a cuvette and illuminated from above with light of the required wavelength for a predetermined period of time. The sample was then removed from the light and was mixed well before the absorbance spectrum was collected using a Hewlett Packard 8452A diode array UV-Vis spectrophotometer. This procedure was repeated for various illumination times until no further change in the sample absorbance was observed. The spectra collected at various times were analyzed and used to generate the concentration versus time plots. The experimental procedure adopted for all the initiators was the same.

#### **4.4. Development of the Model**

The spatial and temporal evolution of the light intensity gradient as well as the concentration gradients of the initiator and the photolysis products are described by the following set of coupled differential equations (see Appendix, section 1 and 2 for derivation). Here,  $I(z,t)$  represents the light intensity at time 't' and at a depth 'z' below the sample surface.  $C_i(z,t)$  represents the photoinitiator concentration and  $C_A(z,t)$ ,  $C_B(z,t)$  etc. represent the concentrations of the photolysis products 'A', 'B' etc.

$$\frac{\partial I(z,t)}{\partial z} = -[S + k_i C_i(z,t) + k_A C_A(z,t) + k_B C_B(z,t) + \dots] I(z,t) \quad (4.1)$$

$$\frac{\partial C_i(z,t)}{\partial t} = -\left(\frac{k_i}{N_A h \nu}\right) \phi_i I(z,t) C_i(z,t) + D_i \frac{\partial^2 C_i(z,t)}{\partial z^2} \quad (4.2)$$

$$\frac{\partial C_A(z,t)}{\partial t} = \left(\frac{k_i}{N_A h \nu}\right) \phi_A I(z,t) C_i(z,t) + D_A \frac{\partial^2 C_A(z,t)}{\partial z^2} \quad (4.3)$$

$$\frac{\partial C_B(z,t)}{\partial t} = \left(\frac{k_i}{N_A h \nu}\right) \phi_B I(z,t) C_i(z,t) + D_B \frac{\partial^2 C_B(z,t)}{\partial z^2} \quad (4.4)$$

*etc.*

$$\begin{aligned} \text{Initial Conditions: } C_i(z,0) &= C_{i_0} \\ C_A(z,0) &= 0 \\ C_B(z,0) &= 0 \end{aligned}$$

*etc.*

$$\text{Boundary Condition: } I(0,t) = I_0$$

The above equations are a set of coupled second order partial differential equations which are difficult to solve. However, if the effect of diffusion is neglected (as justified in section 4.6), then they can be simplified to the following form.

$$\frac{\partial I}{\partial z} = -\alpha C_{i_0} I - \beta C_i I \quad (4.5)$$

$$\frac{\partial C}{\partial t} = -\gamma I_0 I C_i \quad (4.6)$$

$$I(t,0) = 1$$

$$C_i(0,z) = C_{i_0}$$

Where,

$$\alpha = \left[ \frac{S}{C_{io}} + \left( \frac{k_A \phi_A + k_B \phi_B + \dots}{\phi_i} \right) \right] \quad (4.7)$$

$$\beta = \left[ \frac{k_i \phi_i - (k_A \phi_A + k_B \phi_B + \dots)}{\phi_i} \right] \quad (4.8)$$

and

$$\gamma = \left( \frac{k_i \phi_i}{N_A h \nu} \right) \quad (4.9)$$

This set of coupled first order partial differential equations can be further reduced to an ordinary differential equation shown below

$$\frac{dc}{dt} = -\alpha C_{io} c + \beta C_{io} (e^{-c} - 1) \quad \text{where } c = \ln(C_{io}/C_i) \quad (4.10)$$

$$@ z = 0, c = \gamma I_0 t$$

The constants  $\alpha$  and  $\beta$  can be determined from a single photobleaching experiment as follows (see appendix, section 3 for derivation)

$$\alpha = -\frac{1}{C_{io} l} \ln(T_\infty) \quad (4.11)$$

$$\beta = \frac{1}{C_{io} l} \ln\left(\frac{T_\infty}{T_0}\right) \quad (4.12)$$

where  $T_0$  is the initial transmittance and  $T_\infty$  is the final transmittance (after complete bleaching) of a thickness 'l' of the sample at the wavelength being considered.

Equation (4.10) can be solved numerically to obtain  $c$  as a function of  $z$  at different times. From this information, it is possible to obtain the initiator concentration in the sample as well as the light intensity in the sample as a function of time and sample depth.

The experimental data obtained is a plot of the average photoinitiator concentration in the sample as a function of time. In order to obtain this information from the model, the concentration curve at that time must be integrated through the entire sample depth. This is easily accomplished using numerical integration techniques

## **4.5. Results and Discussion**

### *Simulation Results*

Figures 4.2 and 4.3 show the simulation results for evolution of light intensity gradient in the photoinitiator solution with time. It can be seen that the severity of the intensity gradient gradually reduces with time until it becomes constant (no longer changing with time). The ultimate intensity gradient reached depends upon the absorbance of the photolysis products. If the products are non absorbing at the wavelength being considered then the gradient is completely eliminated (Figure 4.2). However, if the products of photolysis do absorb at the wavelength of interest, then the gradient is partially eliminated as shown in Figure 4.3. Figures 4.4, 4.5 and 4.6 show the change the transmittance of the photoinitiator solution with time for different sample thickness. It is clear that at larger sample depths, the curve has a characteristic sigmoidal shape, indicating an initial lag or induction period before the intensity begins to increase

rapidly. Figure 4.7 shows the effect of solvent absorbance on the gradient elimination rate. It is clear that even a small extinction coefficient of the solvent at the wavelength of interest has a considerable effect on the gradient elimination rate because the solvent constitutes more than 99% of the photoinitiator solution.

### *Experimental Verification of Model*

The method adopted for experimental verification of the model is described below. The photoinitiator solution was irradiated from above for a predetermined period of time. The solution was then well stirred and its absorbance spectrum is taken. From the absorbance spectrum, the photoinitiator concentration in the well stirred solution was determined based upon the extinction coefficient of the initiator and the photolysis products (using equation 23 from the appendix). This is the experimental data. The theoretical concentration in the well stirred solution was calculated by integrating the concentration gradient predicted by the model with respect to  $z$  then dividing by the total depth. Thus the model and experiment could be compared.

Figures 4.8 through 4.14 show the comparison of theoretical and experimental results for the monochromatic photobleaching experiments for four photoinitiators at different concentrations, light intensities and thickness. It is seen that the model compares well with experiment in every case. Small deviations could arise because the irradiation was not perfectly monochromatic. It was observed that the value of the constant  $\gamma$  was different from the value which was theoretically predicted by equation 4.9.

This was true for all the photoinitiators studied. Table 4.1 shows the theoretical and actual values of  $\gamma$  for the different photoinitiators which were investigated. It is seen that the actual value is about 1.5 to 2.5 times the theoretically predicted value in all cases. However, for a given photoinitiator and light wavelength, the values of  $\alpha$ ,  $\beta$  and  $\gamma$  are constant and completely characterize the photobleaching of the initiator at that wavelength.

#### 4.6. Effect of Diffusion

##### *Model for Photobleaching Including the Effect of Diffusion*

When the solution of photoinitiator is irradiated from above, the light intensity gradient causes different depths of the sample to undergo bleaching at different rates, thereby resulting in a concentration gradient through the sample depth. The concentration gradient results in diffusion of the photoinitiator, which in turn affects the rate of photobleaching. The following is a brief analysis of the effect of diffusion in the photobleaching process.

Consider a solution of photoinitiator whose photolysis products do not absorb at the wavelength being considered. Then, the equations describing the photobleaching effect including the effect of diffusion are:

$$\frac{\partial I(z,t)}{\partial z} = -k_i C_i(z,t) I(z,t) \quad (4.13)$$

$$\frac{\partial C_i(z,t)}{\partial t} = -\left(\frac{k_i \phi_i}{N_A h \nu}\right) C_i(z,t) + D_i \frac{\partial^2 C_i(z,t)}{\partial z^2} \quad (4.14)$$

the above equations can be transformed into the following (see appendix, section 5)

$$\frac{\partial u}{\partial t} - D_i \frac{\partial^2 u}{\partial z^2} = a(1 - e^u) \quad (4.15)$$

$$\text{where, } u = \ln\left(\frac{I}{I_0}\right) \quad (4.16)$$

$$\text{and, } a = \left(\frac{k_i \phi_i I_0}{N_A h \nu}\right) \quad (4.17)$$

The initial and boundary conditions are

$$\begin{aligned} @ z = 0, u &= 0 \\ @ t = 0, u &= -k_i C_{i0} z \end{aligned} \quad (4.18)$$

Equation (4.15) was solved numerically using the finite difference method (see appendix, section 5) and the results were compared to the solution without including the effect of diffusion ( $D_i=0$ ). In the simulations discussed in this section, a representative value<sup>8</sup> of diffusion coefficient used was  $10^{-4}$  cm<sup>2</sup>/sec. If anything, this value of diffusion coefficient is high for polymerizing systems. Figure 4.15 illustrates the effect of diffusion on the photobleaching of a dilute solution of benzoin ethyl ether subjected monochromatic light of moderate intensity. It is clear that at small time scales (about 2 minutes), diffusion has practically no effect. However at larger time scales, there is a small but observable effect of diffusion on the bleaching process. Figure 4.16 shows the effect of increasing the light intensity. Increasing the light intensity from 2.8 mW/cm<sup>2</sup> to 10 mW/cm<sup>2</sup> results in a considerably faster bleaching and effect of diffusion is not noticeable during the entire bleaching process. Figure 4.17 illustrates the effect of increasing the photoinitiator concentration. The light intensity used is moderate at 2.8

$\text{mW/cm}^2$  (the same as Figure 4.15). Again, at small time scales, the effect of diffusion is not noticeable however, at larger time scales, the effect of diffusion is very clear and there is a considerable error involved if the diffusion term is neglected. In general, it can be concluded that at large time scales, the effect of diffusion is more pronounced and factors such as low light intensity and high photoinitiator concentration which tend to increase the time scale of photobleaching cause the effect of diffusion to become more important in the analysis.

Figures 4.18 and 4.19 show the effect of diffusion on the photobleaching of BEE under the same conditions (initiator concentration and light intensity) used in the experiment. It is clear that effect of diffusion in this case is quite negligible and hence, neglecting the diffusion term in the photobleaching model is justified. The same conclusion can be drawn for the other photoinitiators based on the time scale of the experiment and the concentration of photoinitiator used.

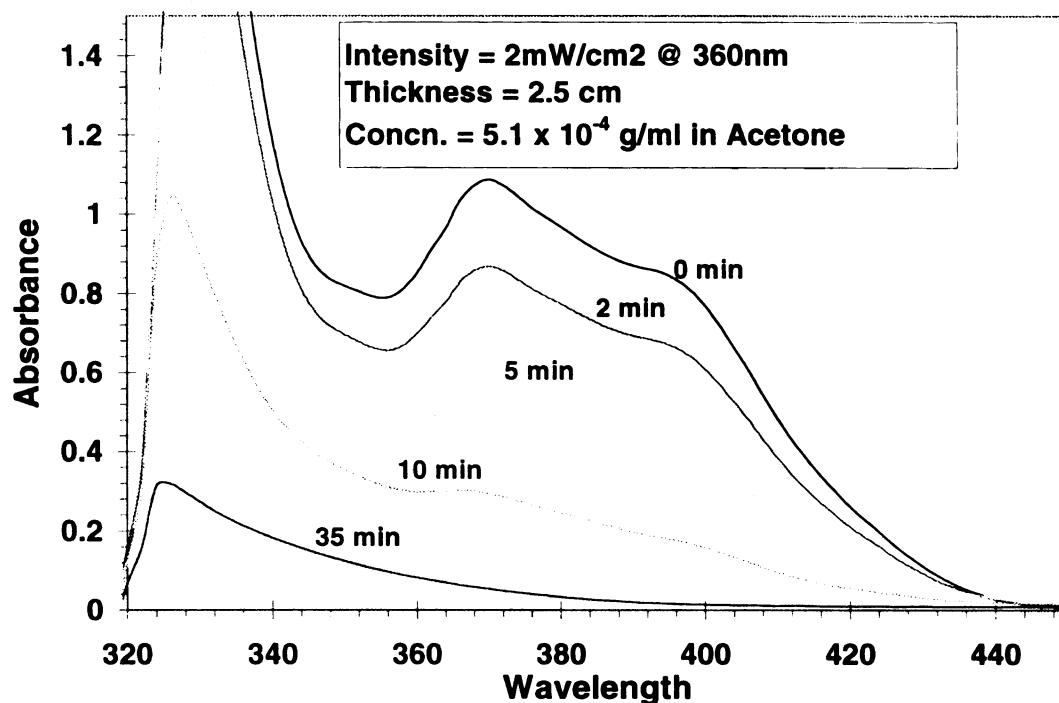
#### *Effect of Diffusion Coefficient*

Figure 4.20 shows the effect of changing the value of the diffusion coefficient on the photobleaching process. There are two limiting cases: (1) no diffusion in the sample (diffusion coefficient = 0) and (2) well mixed sample (effectively infinite diffusion). Analytical solution to the photobleaching equations can be obtained for both these cases (see appendix, sections 6 and 7). The light intensity gradient through the sample for cases involving a finite diffusion coefficient lie in between the two limiting cases as seen in Figure 4.20. As the diffusion coefficient is increased from  $10^{-5} \text{ cm}^2/\text{s}$  to  $10^{-2} \text{ cm}^2/\text{s}$ , the

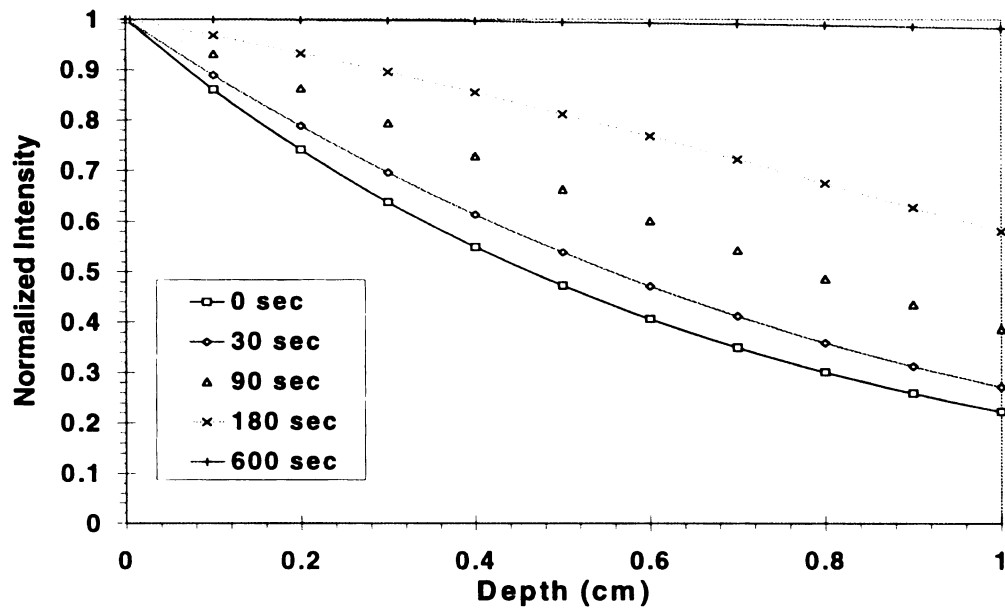
light intensity gradient through the sample shifts from one approaching the no diffusion limiting case towards the well mixed sample limiting case (note that curve for  $10^{-2} \text{ cm}^2/\text{s}$  case almost coincides with the curve for the well mixed case).

#### **4.7. Conclusions**

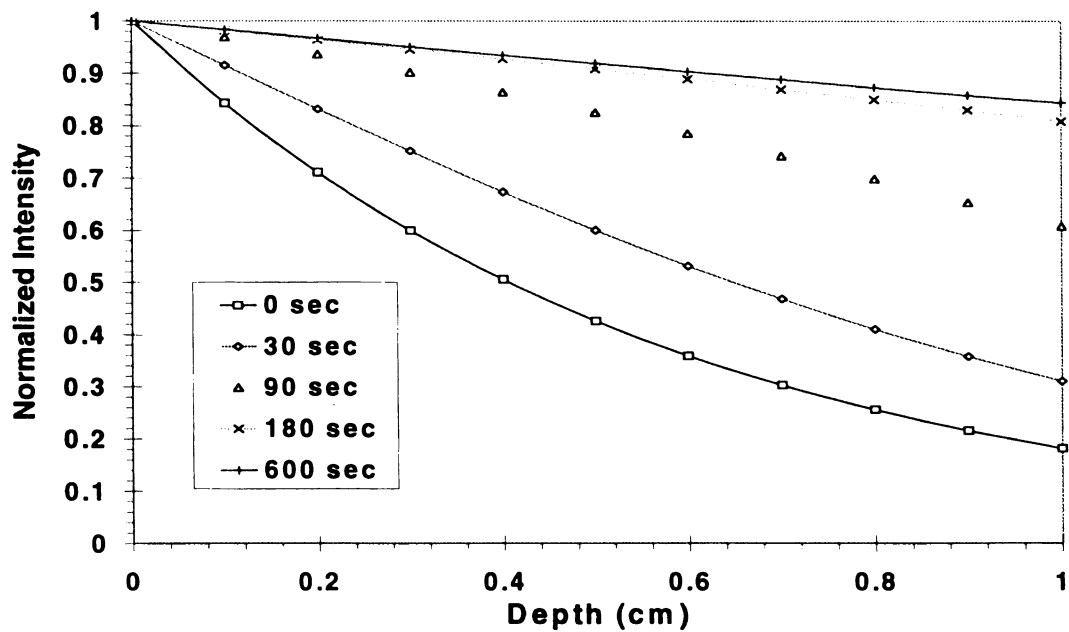
A mathematical model was developed to characterize the photobleaching of photoinitiators. The model contains three constants which can easily be determined experimentally and completely characterize the photobleaching for a given initiator and wavelength of light. The model was verified experimentally and good agreement between theory and experiment was found. The effect of diffusion on the photobleaching was shown and it was demonstrated that diffusion does not have a significant effect under the conditions studied. The model can be used to compare the photobleaching effectiveness of different initiators and thereby in making a choice of initiator for curing systems where the depth of cure is a major concern. For example, Figure 4.21 compares the photobleaching rate of two initiators namely BEE and BAPO. Obviously, BAPO bleaches faster than BEE, thereby making it a better choice as a photoinitiator for thick systems.



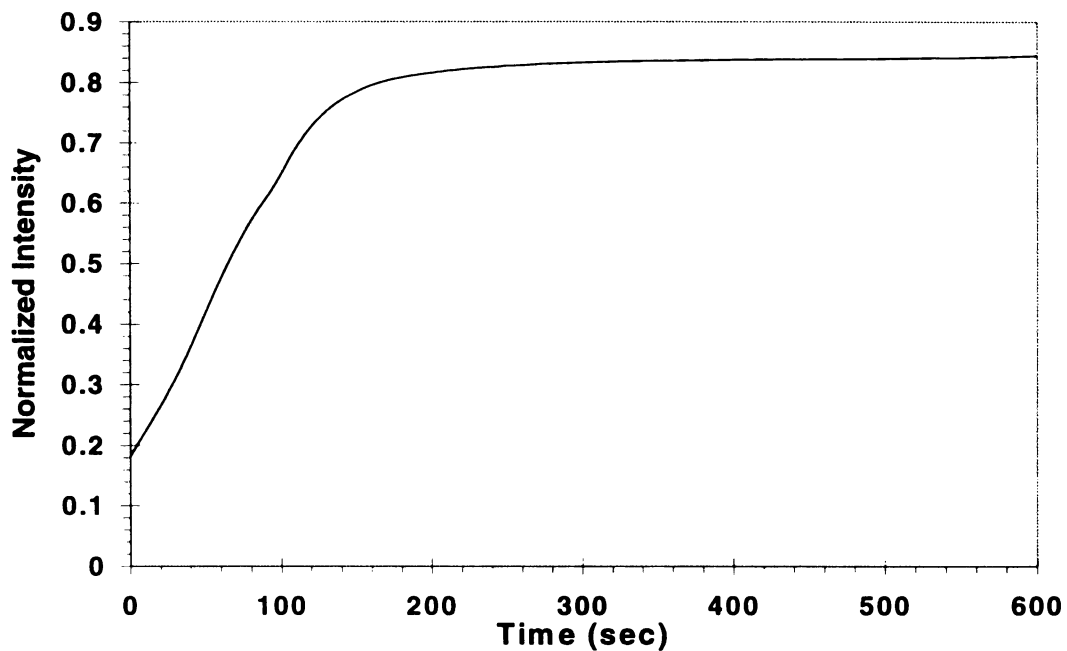
**Figure 4.1.** Time evolution of the absorbance spectrum of a bis-acyl phosphine oxide (BAPO) photoinitiator as it is irradiated with low intensity UV light. The 2.5 cm thick sample containing  $5.1 \times 10^{-4} \text{ g ml}^{-1}$  of the initiator dissolved in acetone was illuminated from above with filtered light from a mercury lamp. The light was passed through a 10 nm bandpass filter centered at 360 nm, and the intensity at the top surface of the sample was  $2 \text{ mW cm}^{-2}$ .



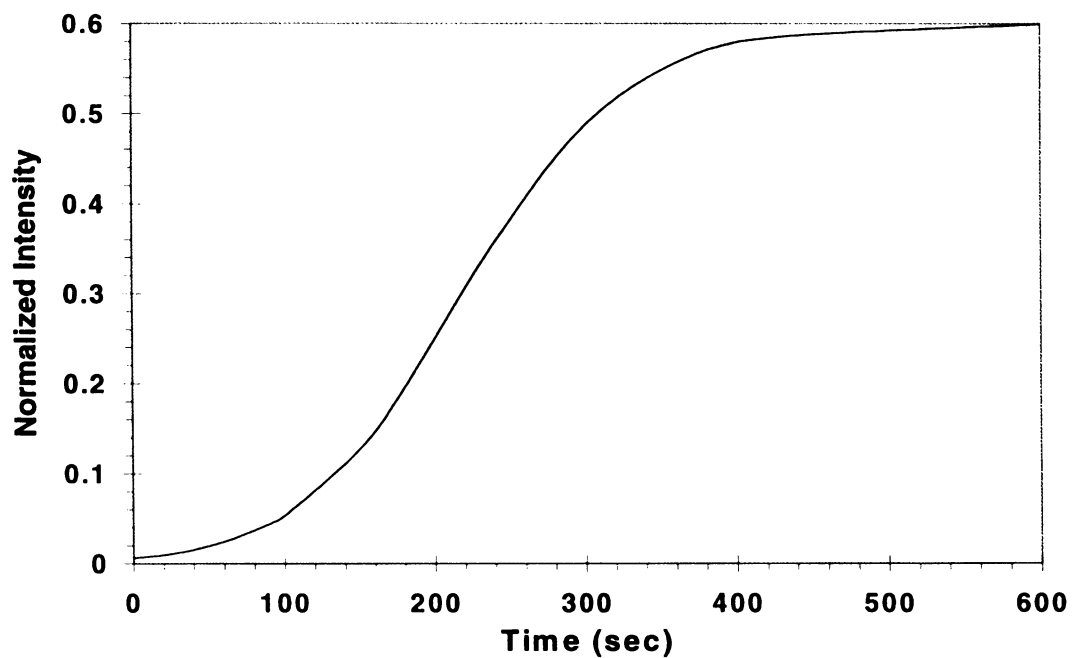
**Figure 4.2.** Elimination of the intensity gradient in a 1cm thick solution of BEE. The concentration of BEE is  $5 \times 10^{-4}$  g/ml and the incident light intensity is  $5 \text{ mW/cm}^2$  at 330 nm



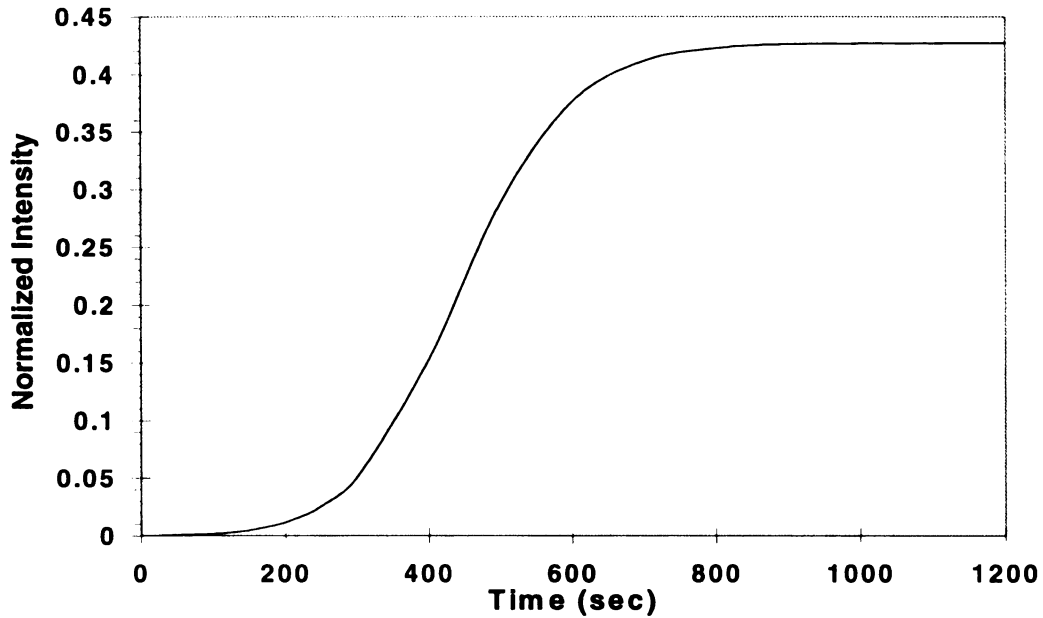
**Figure 4.3.** Elimination of the light intensity gradient in a 1cm thick solution of TPO. The concentration of TPO is  $5 \times 10^{-4}$  g/ml and the incident light intensity is  $5 \text{ mW/cm}^2$  at 360nm



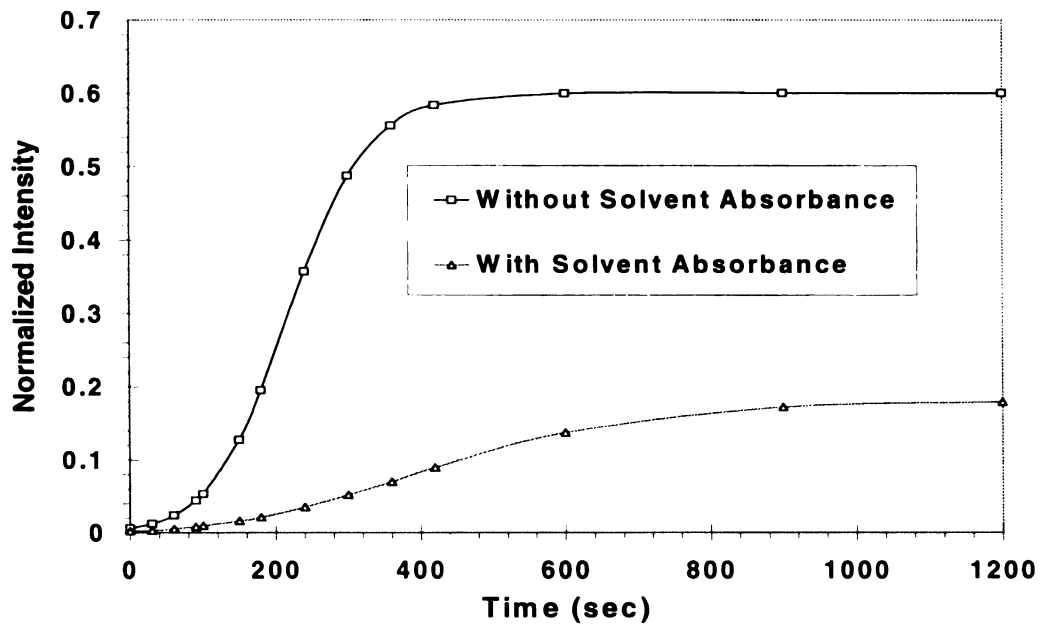
**Figure 4.4.** Change in transmittance as a function of time for a 1cm thick solution of TPO irradiated with 360nm light of intensity  $5 \text{ mW/cm}^2$



**Figure 4.5.** Change in transmittance as a function of time for a 3cm thick solution of TPO irradiated with 360nm light of intensity  $5 \text{ mW/cm}^2$



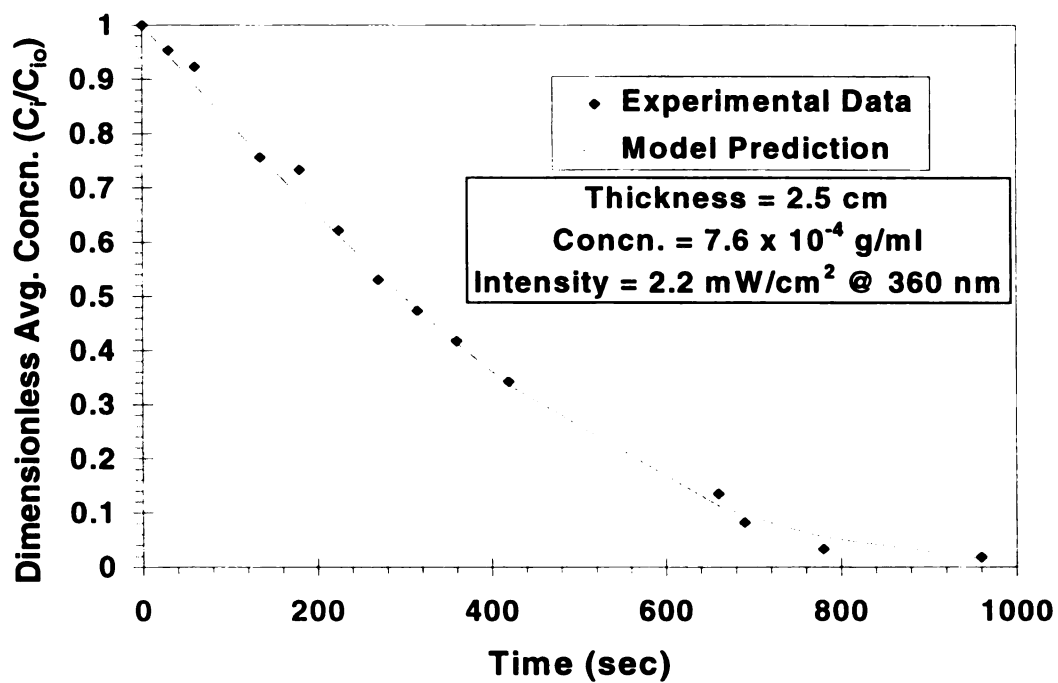
**Figure 4.6.** Change in transmittance as a function of time for a 5cm thick solution of TPO irradiated with 360 nm light of intensity  $5 \text{ mW/cm}^2$



**Figure 4.7.** Effect of solvent absorbance on the evolution of the transmittance of a 3cm thick solution of TPO in a solvent with an extinction coefficient of  $0.5 \text{ ml/g.cm}$  and  $0.8 \text{ gm/ml}$  density. The concentration of TPO is  $5 \times 10^{-4} \text{ g/ml}$  and intensity of the incident light is  $5 \text{ mW/cm}^2$

**Table 4.1.** Comparison of theoretical and best fit values of  $\gamma$  for different photoinitiators

Initiator	$\gamma$ (Theoretical)	$\gamma$ (Best Fit)
BAPO	$2.4 \times 10^{-4}$	$2.9 \times 10^{-4}$
TPO	$2.0 \times 10^{-4}$	$5.4 \times 10^{-4}$
BEE	$0.96 \times 10^{-4}$	$1.7 \times 10^{-4}$
Titanocene	$4.6 \times 10^{-4}$	$10 \times 10^{-4}$

**Figure 4.8.** Comparison of theory and experiment for photobleaching of TPO

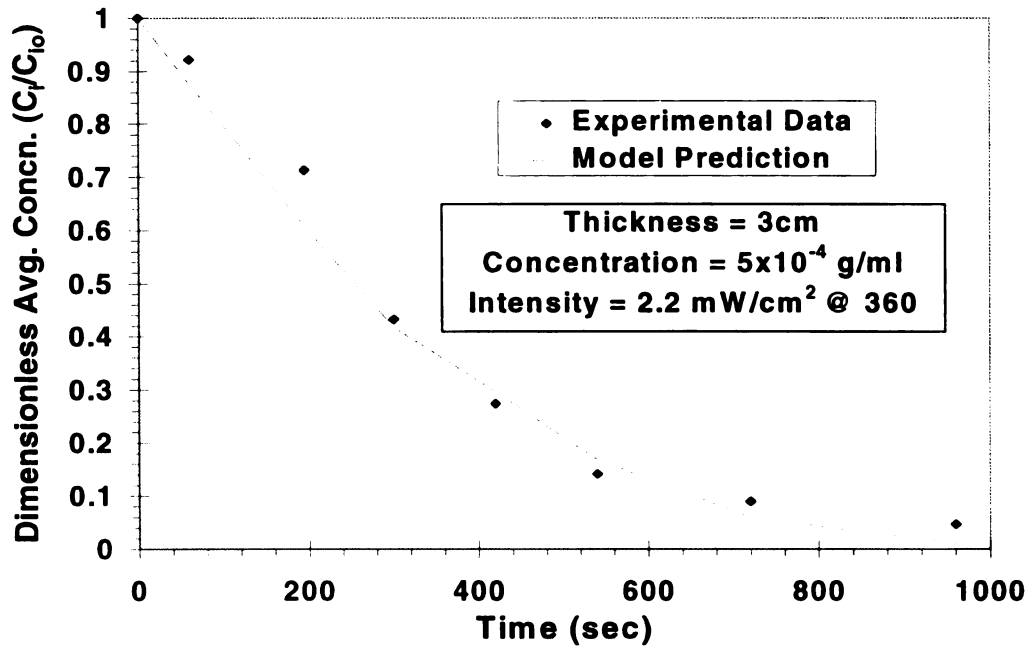


Figure 4.9. Comparison of theory and experiment for the photobleaching of TPO

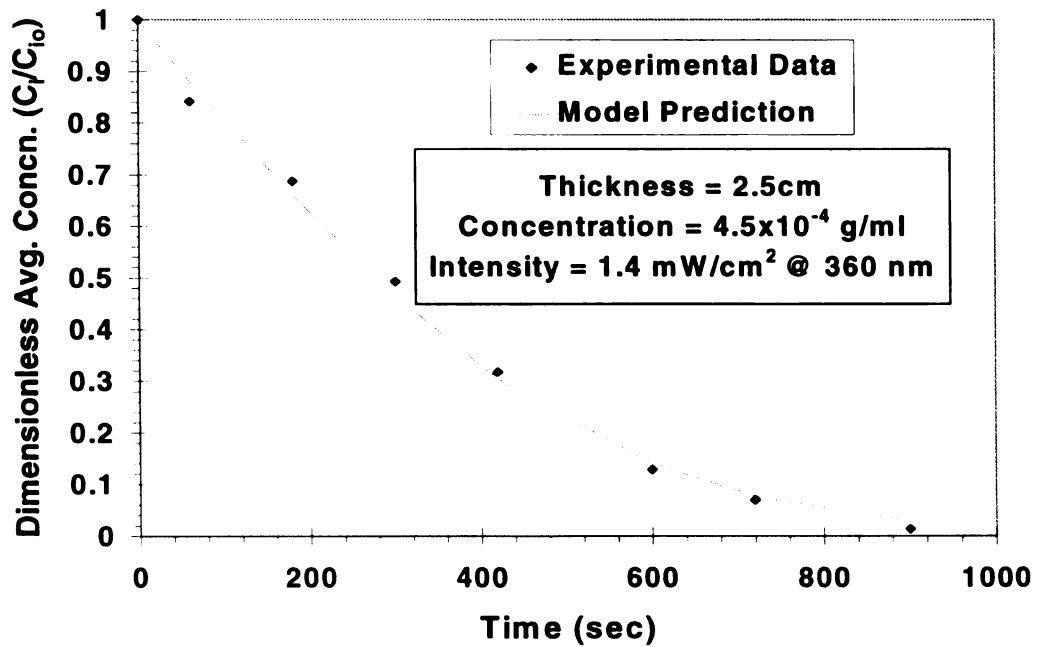


Figure 4.10. Comparison of theory and experiment for the photobleaching of TPO

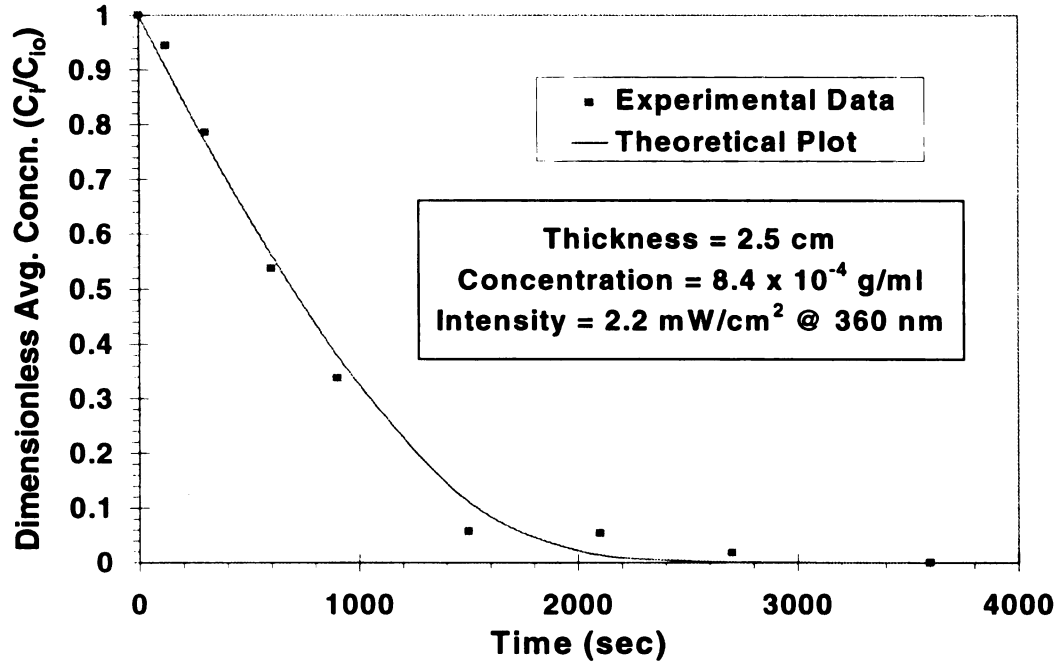


Figure 4.11. Comparison of theory and experiment for the photobleaching of BAPO

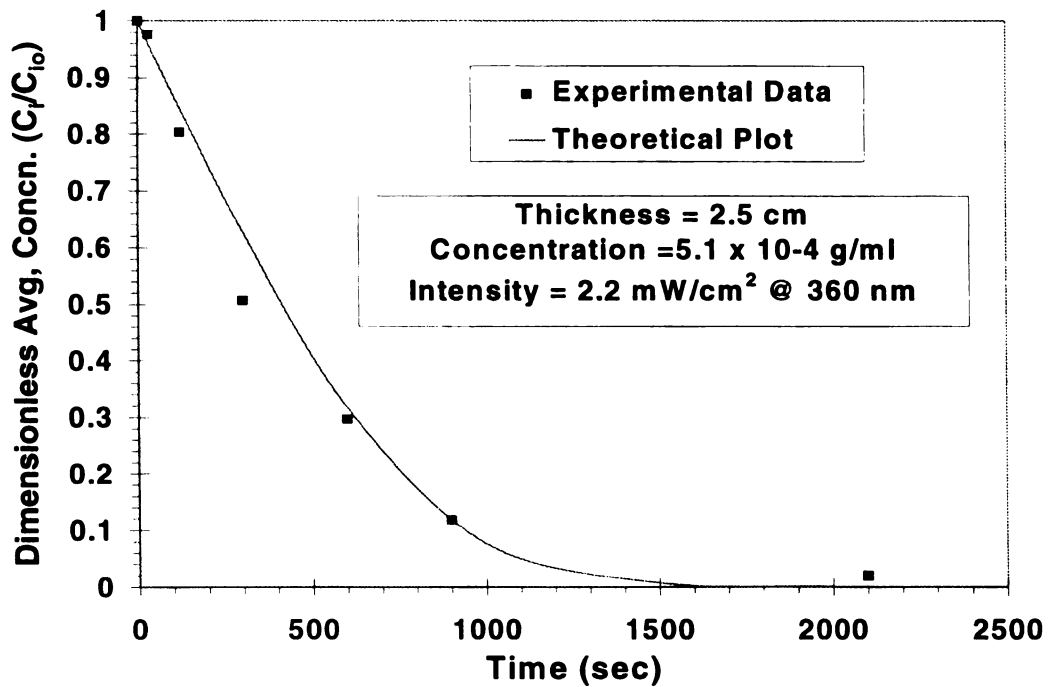


Figure 4.12. Comparison of theory and experiment for the photobleaching of BAPO

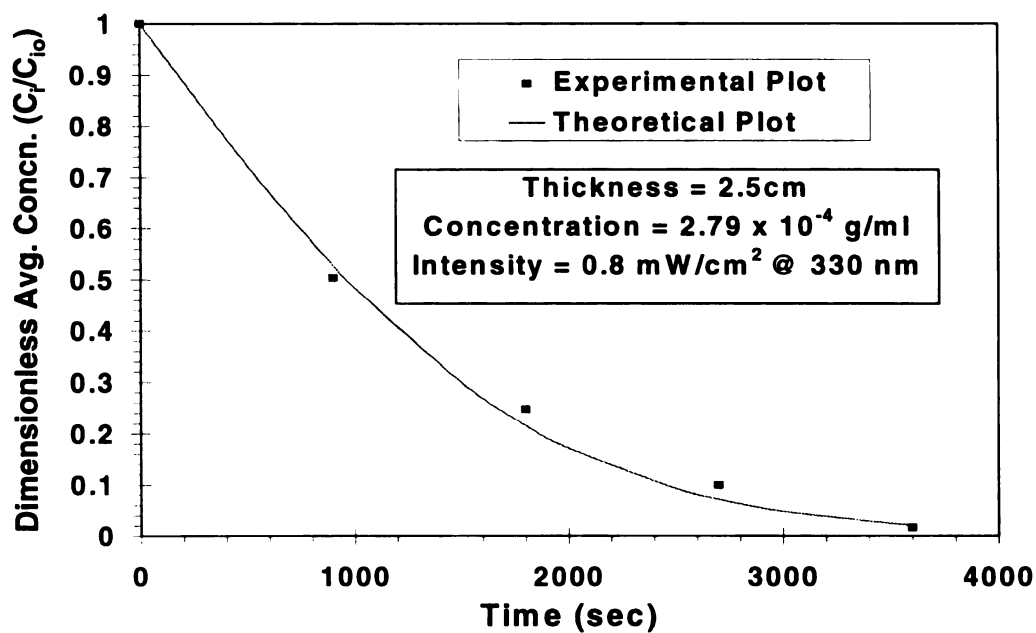


Figure 4.13. Comparison of theory and experiment for the photobleaching of BEE

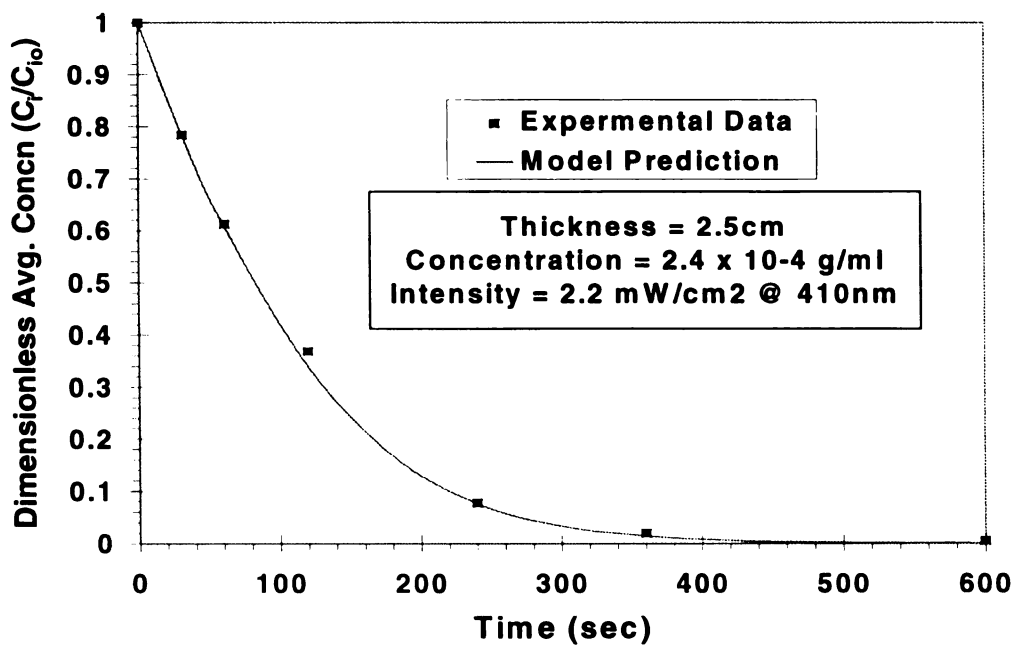
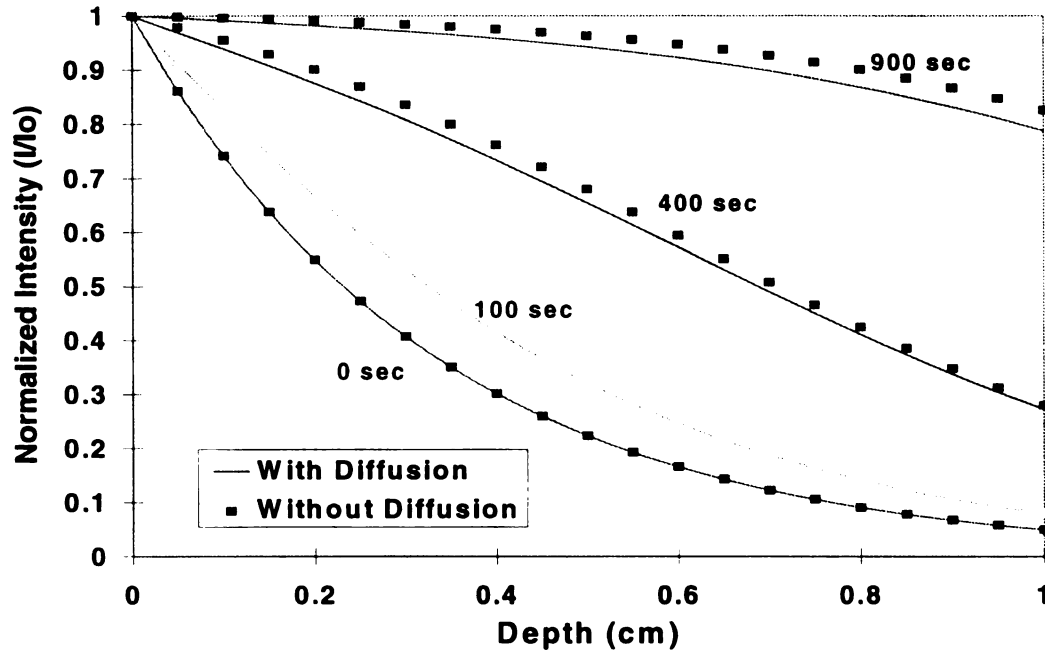
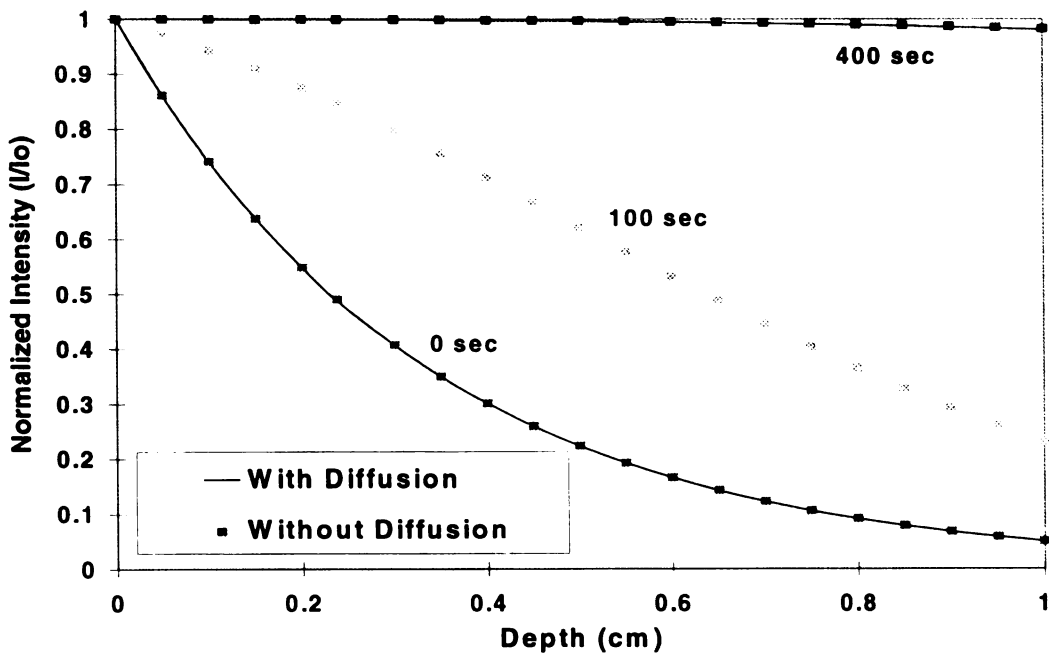


Figure 4.14. Comparison of theory and experiment for photobleaching of substituted titanocene



**Figure 4.15.** Effect of diffusion on the photobleaching rate of BEE. The concentration is  $10^{-3}$  g/ml and the light intensity is  $2.8 \text{ mW/cm}^2$  @ 330nm



**Figure 4.16.** Effect of diffusion on the photobleaching rate of BEE. The concentration is  $10^{-3}$  g/ml and the light intensity is  $10 \text{ mW/cm}^2$  @ 330nm

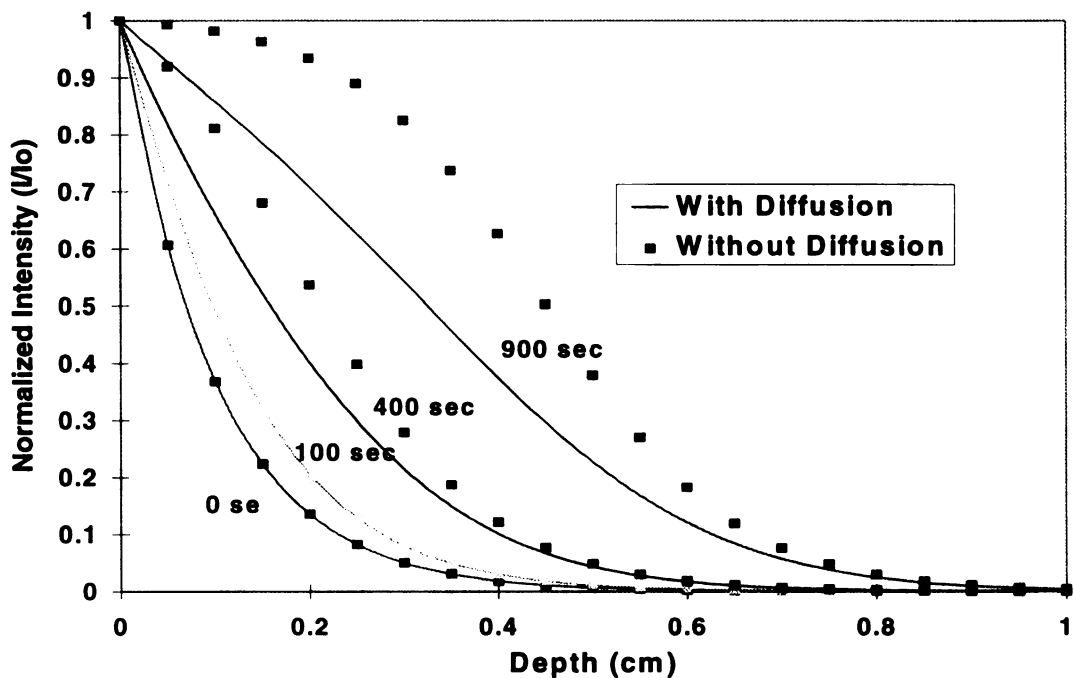


**Figure 4.17.** Effect of diffusion on the photobleaching rate of BEE. The concentration is  $3.3 \times 10^{-3}$  g/ml and the light intensity is  $10 \text{ mW/cm}^2$  @ 330nm

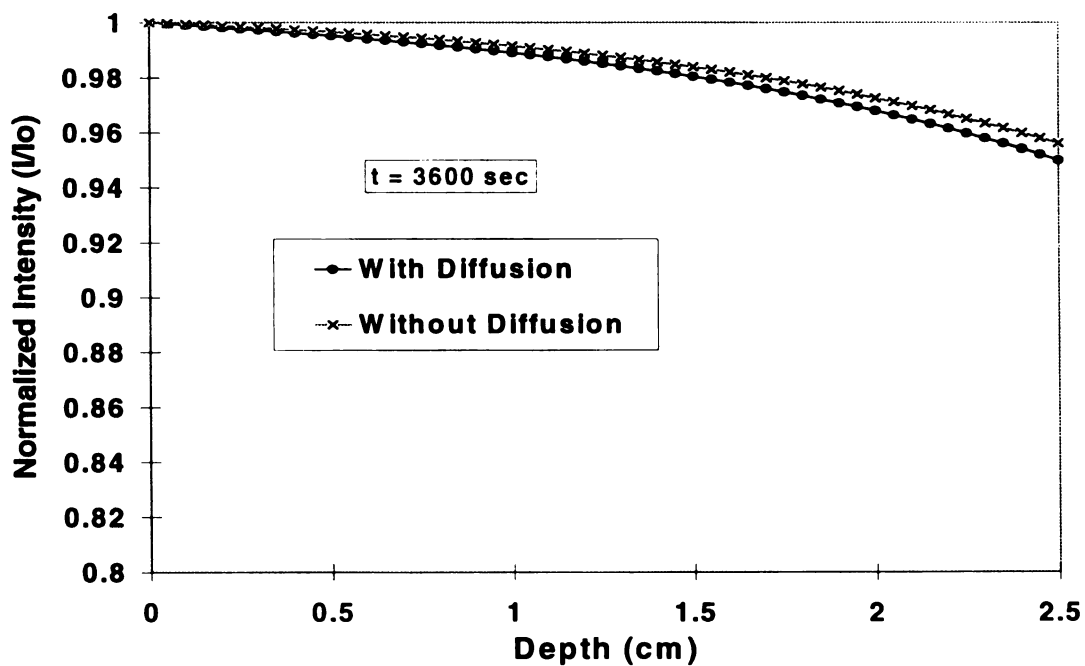


**Figure 4.18.** Effect of diffusion on the photobleaching rate of BEE. The concentration is  $2.79 \times 10^{-4}$  g/ml and the light intensity is  $0.8 \text{ mW/cm}^2$  @ 330nm

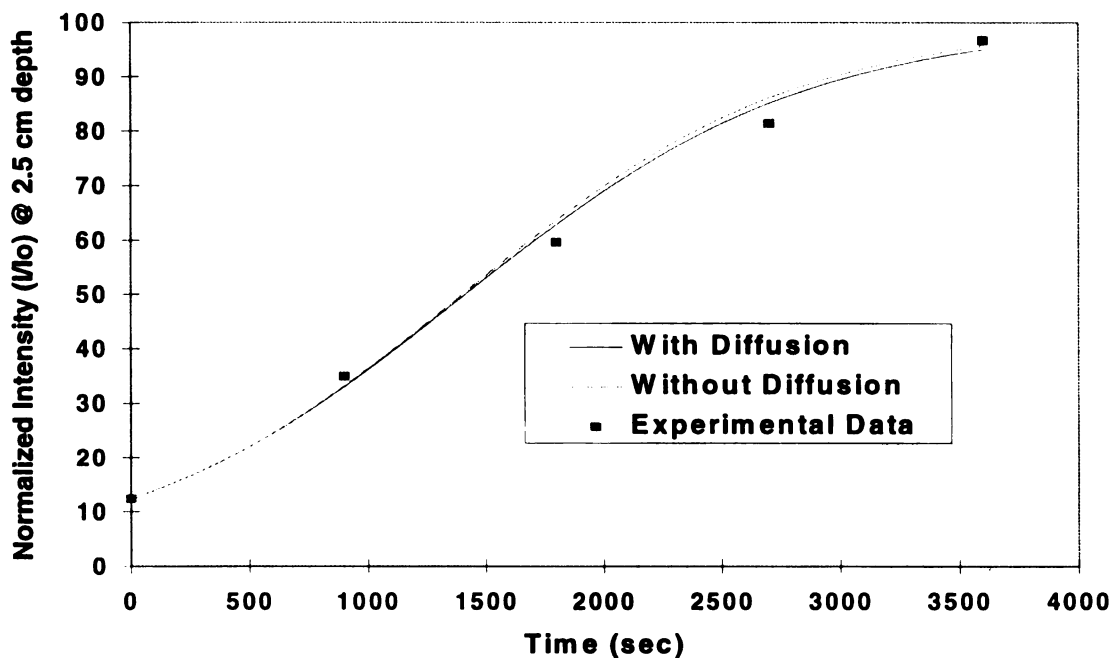


Figure 4.19. Comparison of experimental and model data (with and without diffusion) for the photobleaching of BEE.

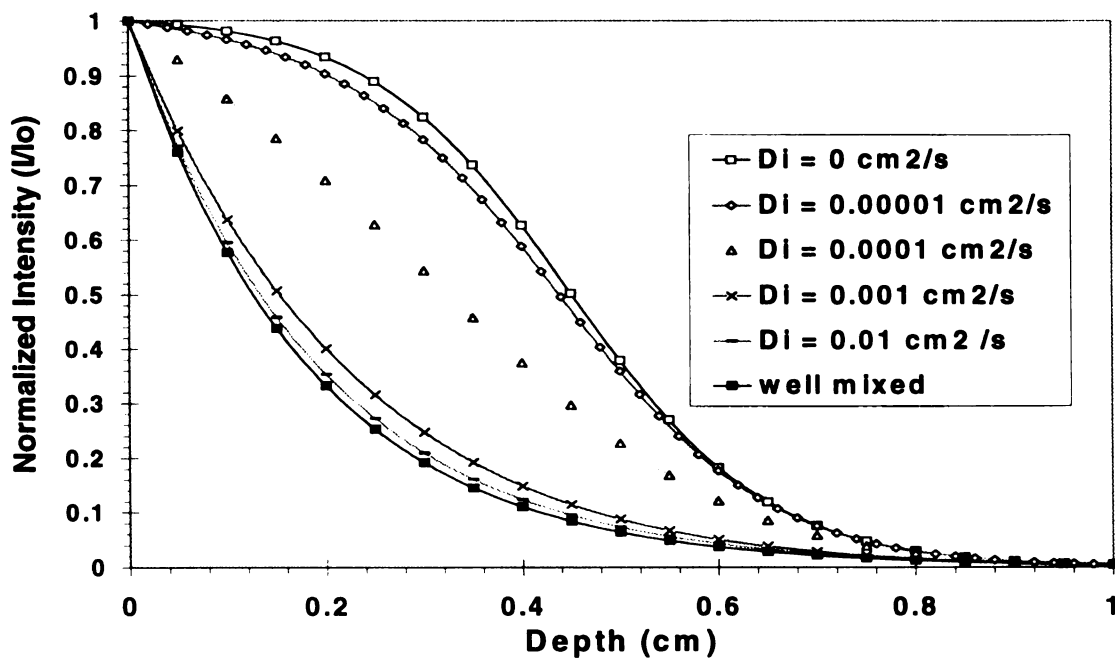
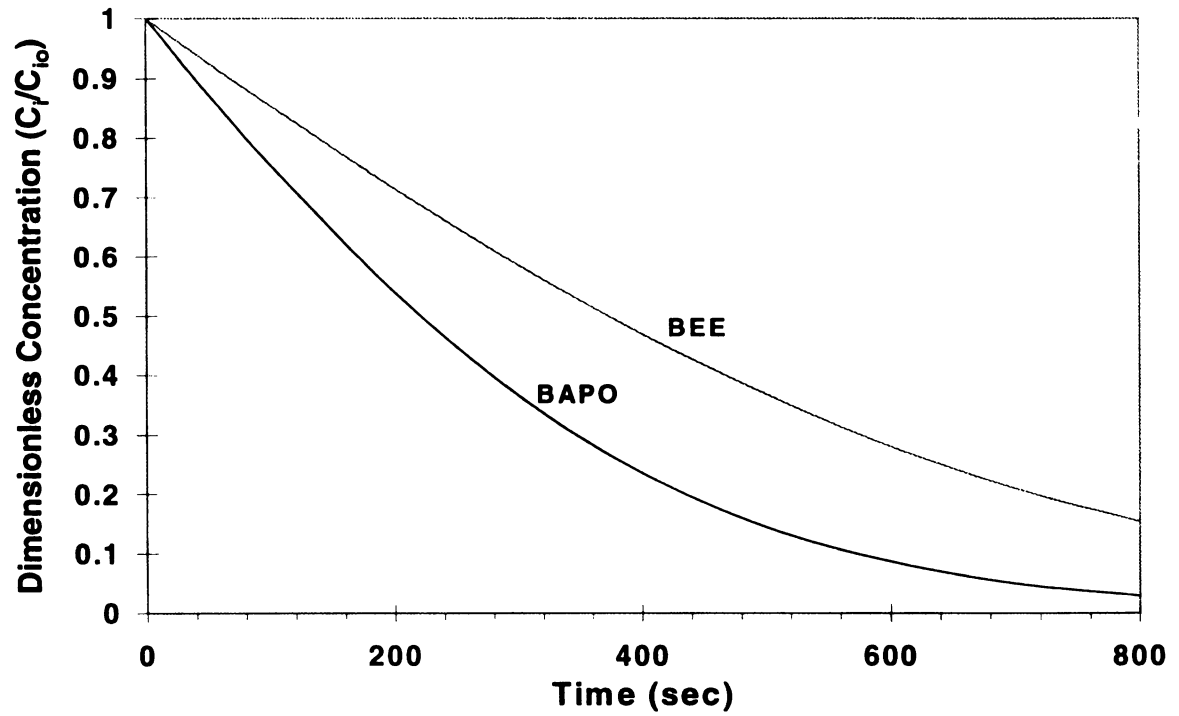


Figure 4.20. Effect of initiator diffusion coefficient on the photobleaching process. The light intensity is  $10 \text{ mW/cm}^2$  and the concentration is  $3.3 \times 10^{-3} \text{ g/ml}$ . All the intensity gradients shown are at time = 900 seconds



**Figure 4.21.** Comparison of the photobleaching rate of BAPO and BEE. Both the solutions had the same initial absorbance of 1 and solution depth of 2 cm. The light intensity used for bleaching was  $2.2 \text{ mW/cm}^2$

#### 4.8. List of References

1. J.D. Coyle, *Introduction to Organic Photochemistry*, John Wiley & Sons, 1986
2. J.P. Fouassier, *Photoinitiation Photopolymerization and Photocuring Fundamentals and Applications*, Hanser Publishers, 1995
3. F.D. Lewis, R.T. Lauterbach, H.G. Heine, W. Hartmann, H. Rudolph, *J. Am. Chem. Soc.*, **97**, 1519, 1975
4. K. Dietliker, G. Hug, R. Kaeser, M. Kohler, U. Kolczak, D. Leppard, L. Misev, G. Rist, W. Rutsch, *Novel High Performance Bisacylphosphine Oxide (BAPO) Photoinitiators*, Ciba-Geigy Corporation, 1994
5. J. Finter, M. Riediker, O. Rohde, B. Rotzinger, *Makromol. Chem., Macromol. Symp.*, **24**, 177 1989
6. K. Dietliker, In *Radiation Curing in Polymer Science and Technology*, Volume II, J.P. Fouassier and J.F. Rabek, Eds., Elsevier Applied Science, pp.155-237,1993
7. L.S. Coons, B. Rangarajan, D. Godshall, A.B. Scranton, *ACS Symposium Series*, in press
8. R.E. Emmert, R.L. Pigford, *Chemical Engineers' Handbook*, 4<sup>th</sup> Ed., R.H. Perry, C.H. Chilton and S.Y. Kirkpatrick, Eds., McGraw-Hill, pp. 14.22 - 14.23

### 4.9. List of Symbols

$C_A$	Concentration of photolysis product 'A' in solution
$C_B$	Concentration of photolysis product 'B' in solution
$C_i$	Concentration of initiator
$C_{i0}$	Initial concentration of initiator solution
$D_i$	Diffusion coefficient of initiator in solvent
$c$	$\ln(C_{i0}/C_i)$
$h$	Plancks Constant
$I$	Intensity of light at the wavelength being considered
$I_0$	Intensity of light at sample surface
$k_A$	Extinction coefficient of species 'A' in solution multiplied by 2.303
$k_B$	Extinction coefficient of species 'B' in solution multiplied by 2.303
$k_i$	Extinction coefficient of initiator in solution multiplied by 2.303
$N_A$	Avogadro number
$t$	Time variable
$S$	Absorbance of the solvent divided by the path length
$T_0$	Transmittance of sample at time 0
$T_\infty$	Transmittance of sample at time $\infty$
$z$	Depth (distance) variable
$\alpha, \beta, \gamma$	Constants
$\phi_A$	Quantum yield of species 'A'
$\phi_B$	Quantum yield of species 'B'
$\phi_i$	Quantum yield of photolysis of initiator
$\nu$	Frequency of light being used

#### 4.10. Appendix

##### 1. Assumptions made in the derivation

1. The photoinitiator solution is dilute, hence Beer-Lambert's law is valid
2. The incident light is monochromatic
3. There are no secondary, thermally driven chemical reactions in which the photoinitiator participates

##### 2. Derivation of the Model Equations

The initial concentration of the photoinitiator solution is  $C_{i0}$  and the intensity of light at the surface of the solution at that wavelength is  $I \text{ W/m}^2$ . Consider a thin layer of solution of thickness  $\delta z$  at a depth  $z$  from the surface. The number of photons striking this surface in a small time  $\delta t$  is given by

$$i = \frac{aI\delta t}{h\nu} \quad (1)$$

The number of photons absorbed by any species 'S' present in the solution is given by

$$(N_A C_s a \delta z) k_s i \quad (2)$$

The total number of photons absorbed is the sum of the photons absorbed by each of the species present in the solution which includes the solvent itself. Hence, change in the number of photons passing through the thickness  $dz$  of the solution is given by

$$\delta i = (N_A a \delta x) (S + k_i C_i + k_A C_A + k_B C_B + \dots) \quad (3)$$

So, from equations (1), (2) and (3), we have

$$\frac{a \delta I \delta x}{h \nu} = N_A a \delta x \frac{a I \delta x}{h \nu} \left[ S + k_i C_i + k_A C_A + k_B C_B + \dots \right] \quad (4)$$

hence taking limits in equation (4), we get

$$\frac{\partial I}{\partial x} = - \left[ S + k_i C_i + k_A C_A + k_B C_B + \dots \right] I \quad (5)$$

In the small time  $\delta t$ , the number of molecules of product A that will be formed is given by

$$\delta A = \phi_A [N_A C_i a \delta x] i k_i \quad (6)$$

Due to difference in light intensities at different depths, the concentration of A will also be different. This difference in concentration will cause diffusion of A which must also be accounted for in the model. A molar balance for species A in the differential volume  $adz$  give

$$\delta A = \phi_A [N_A C_i a \delta x] i k_i + N_A J_A a \delta x \Big|_z - N_A J_A a \delta x \Big|_{z+\Delta z} \quad (7)$$

Equation (7) can be simplified by using Fick's Law for diffusion and taking the limits to give

$$\frac{\partial C_A}{\partial t} = \left( \frac{k_A}{N_A h \nu} \right) \phi_A I C_i + D_A \frac{\partial^2 C_A}{\partial z^2} \quad (8)$$

Similar equations can be written for the species B, C etc., that are formed during the process as shown

$$\frac{\partial C_B}{\partial t} = \left( \frac{k_B}{N_A h \nu} \right) \phi_B I C_i + D_B \frac{\partial^2 C_B}{\partial z^2} \quad (9)$$

and so on.

For the initiator, the equation becomes

$$\frac{\partial C_i}{\partial t} = - \left( \frac{k_i}{N_A h \nu} \right) \phi_i I C_i + D_i \frac{\partial^2 C_i}{\partial z^2} \quad (10)$$

Equations (5), (8), (9), (10) together give the final form of the equations describing the effect.

### 3. Determination of constants $\alpha$ and $\beta$

We have

$$\frac{\partial \ln I}{\partial z} = -\alpha C_{i0} - \beta C_i \quad (11)$$

this equation can be rewritten as

$$\frac{\partial \ln T}{\partial z} = -\alpha C_{i0} - \beta C_i \quad (12)$$

where  $T = I/I_0$ .

Hence,

$$T = \exp \left[ -\alpha C_{i0} z - \beta \int_0^z C_i dz \right] \quad (13)$$

using the condition that at  $t=0$ ,  $C_i=C_{i0}$

$$T_0 = \exp \left[ -\alpha C_{i0} z - \beta C_{i0} z \right] \quad (14)$$

using the second condition that at  $t \rightarrow \infty$ ,  $C_i=0$  we get

$$T_\infty = \exp \left[ -\alpha C_{i0} z \right] \quad (15)$$

Equations (14) and (15) can be solved to obtain  $\alpha$  and  $\beta$  as shown in equations (11) and (12) in the paper.

#### 4. Determination of Initiator Concentration from Absorbance Measurement

After the sample has been irradiated for a fixed period of time and well stirred, its absorbance is measured at the wavelength of interest in order to determine the concentration of the remaining (undissociated) photoinitiator. The absorbance of the sample measured experimentally is actually the sum of the absorbance due to the photoinitiator and the products of photolysis. The following analysis separates out the absorbance due to the photolysis products and leads to the equation that is used to determine the photoinitiator concentration from the absorbance data.

Let  $C_{pf}$  be the final concentration (lumped) of all the photolysis products,  $\epsilon_f$  be the lumped extinction coefficient of the photolysis products.  $A_\infty$  is the final absorbance (at  $t \rightarrow \infty$ ) of the photoinitiator solution and 'b' is the path length used in the absorbance measurements. Then

$$A_\infty = \epsilon_f C_{pf} b \quad (16)$$

The final concentration of the photolysis products is given by

$$C_{pf} = C_{i0} \frac{(\phi_A M_A + \phi_B M_B + \dots)}{\phi_i M_i} \quad (17)$$

Where  $M_A$ ,  $M_B$ ,  $M_i$  are the molecular weights of species A, B and I respectively. Hence, from equations (16) and (17),

$$A_\infty = \epsilon_p C_{i0} b \quad (18)$$

where,

$$\epsilon_p = \epsilon_f \frac{(\phi_A M_A + \phi_B M_B + \dots)}{\phi_i M_i} \quad (19)$$

If 'A' is the average absorbance of the solution at the wavelength being considered after it has been irradiated for some time, 't' then we can write

$$A = \varepsilon_j C_p b + \varepsilon_i C_i b \quad (20)$$

where  $C_p$  is the concentration of the photolysis products in the solution.

$$C_p = (C_{i0} - C_i) \frac{(\phi_A M_A + \phi_B M_B + \dots)}{\phi_i M_i} \quad (21)$$

from equations (19), (20) and (21), we get

$$A = \varepsilon_p (C_{i0} - C_i) b + \varepsilon_i C_i b \quad (22)$$

so the final equation for  $C_i$  (photoinitiator concentration) is

$$C_i = \frac{A - \varepsilon_p C_{i0} b}{(\varepsilon_i - \varepsilon_p) b} \quad (23)$$

the constant  $\varepsilon_p$  is found from equation (18) using the experimentally determined value of  $A_{\infty}$ .

### 5. Solution of the Simultaneous Diffusion with Photobleaching Equations

The equations describing the photobleaching effect including the effect of diffusion are (assuming no absorption of the photolysis products at the wavelength of interest:

$$\frac{\partial I}{\partial z} = -k_i C_i I \quad (24)$$

$$\frac{\partial C_i}{\partial t} = -\left(\frac{k_i \phi_i}{N_A h \nu}\right) C_i + D_i \frac{\partial^2 C_i}{\partial z^2} \quad (25)$$

Equation (1) can also be written as

$$C_i = -\frac{1}{k_i} \frac{\partial \ln I}{\partial z} \quad (26)$$

Substituting this in Equation (2), we get the following:

$$\frac{\partial^2 \ln I}{\partial z \partial t} = -\left(\frac{k_i \phi_i}{N_A h \nu}\right) I \left(-\frac{\partial \ln I}{\partial z}\right) + D_i \frac{\partial^3 \ln I}{\partial z^3} \quad (27)$$

Integrating this with respect to  $z$  and using the fact that  $I=I_0$  at  $z=0$ , equation (4) can be reduced to:

$$\frac{\partial \ln I}{\partial t} - D_i \frac{\partial^2 \ln I}{\partial z^2} = \left(\frac{k_i \phi_i}{N_A h \nu}\right) (I_0 - I) \quad (28)$$

which can be finally transformed into

$$\frac{\partial u}{\partial t} - D_i \frac{\partial^2 u}{\partial z^2} = a(1 - e^u) \quad (29)$$

$$\text{where, } u = \ln\left(\frac{I}{I_0}\right) \quad (30)$$

$$\text{and, } a = \left(\frac{k_i \phi_i I_0}{N_A h \nu}\right) \quad (31)$$

with the following initial and boundary conditions

$$\begin{aligned}
& @ z = 0, u = 0 \\
& @ t = 0, u = -k_i C_{i0} z
\end{aligned} \tag{32}$$

using the usual Taylor's series approximations for the derivatives, the finite difference solution scheme for Equation (6) can be written as

$$u_{j,k+1} = (\Delta t) \alpha (1 - e^{-u_{j,k}}) + \frac{D_i(\Delta t)}{(\Delta z)^2} (u_{j-1,k} - 2u_{j,k} + u_{j+1,k}) \tag{33}$$

for all the simulations involving  $D_i = 10^{-4} \text{ cm}^2/\text{sec}$ , the following step sizes were used

$\Delta t = 4 \text{ sec}$ ,  $\Delta z = 0.05 \text{ cm}$ , so that  $\frac{D_i(\Delta t)}{(\Delta z)^2} = 0.16$  which is the optimum value of this ratio

and gives superior accuracy.

#### 6. Analytical solution for the 'no diffusion' case

Putting  $D_i = 0$  in equations (1) and (2) above, we get

$$\frac{\partial I}{\partial z} = -k_i C_i I \tag{34}$$

$$\frac{\partial C_i}{\partial t} = -\left( \frac{k_i \phi_i}{N_A h \nu} \right) C_i \tag{35}$$

then, following the same steps as shown previously, equation (6) becomes

$$\frac{\partial u}{\partial t} = a(1 - e^u) \quad (36)$$

This equation can be solved analytically and the solution is:

$$\frac{I}{I_0} = \frac{1}{e^{az-bt} - e^{-bt} + 1} \quad (37)$$

### 7. Analytical Solution for the 'well mixed' case

Assume that the depth of the photoinitiator solution is L cm and it is always well mixed in the sense that the concentration of the solution does not vary with depth at any given time.

The photobleaching equations then are:

$$I = I_0 e^{-k_i C_i L} \quad (38)$$

$$\frac{dC_i}{dt} = (I - I_0) \left( \frac{\phi_i}{N_A h \nu L} \right) \quad (39)$$

where 'I' is the intensity at the depth 'L' of the sample, and I<sub>0</sub> is the intensity of the initiating light at the top of the sample.

Substituting for I from equation (1), we get a ordinary differential equation for C<sub>i</sub> which can easily be solved. The solution is given by

$$C_i = \frac{1}{k_i L} \ln(e^{aL-bt} - e^{-bt} + 1) \quad (40)$$

so, the equation for the intensity gradient through the sample is

$$\frac{I}{I_0} = (e^{aL-bt} - e^{-bt} + 1)^{-1/L} \quad (41)$$

## **Chapter 5**

# **Investigation of Photoinitiating Systems for Photopolymerization of Composites**

### **Abstract**

Studies were performed to evaluate the suitability of a variety of photoinitiators for UV curing of thick polymer and composite parts. A preliminary choice of photoinitiators was made based upon their absorption spectra, the emission spectrum of the UV light source and the transmittance of the resin. For each photoinitiator, studies were performed to determine the effect of light intensity, photoinitiator concentration and sample thickness on the cure time of the resins. Hybrid photoinitiating systems and dual photo/thermal cure schemes were investigated in an attempt to further reduce the cure time. Finally, composite samples were prepared both by photocuring and by thermal curing and their mechanical properties were evaluated.

### **5.1. Introduction**

The choice of a photoinitiator for curing of thick polymer and composite parts depends on a number of considerations, including spectrum of the initiating light source, absorbance of the monomer and other additives, absorbance and scattering properties of the filler or fiber reinforcement and photoinitiator characteristics such as its absorption spectrum, initiation efficiency and its tendency to photobleach. A preliminary choice of photoinitiator for curing a particular resin can be made based upon the above factors. However, the final choice of photoinitiator must be based upon actual measurements of

the time taken to cure the resin. Determination of cure time can be accomplished by selecting a suitable cure monitoring technique.

Several techniques are available at present for *in situ* cure monitoring of resins. These include infrared spectroscopy, photodifferential scanning calorimetry (PDSC), microwave dielectrometry, viscosity measurements *etc.* Recent reviews in the area of cure monitoring techniques for radiation curing have been published by Davies<sup>1</sup> and Rabek<sup>2</sup>. However, most of these techniques are applicable to thin films. Davies<sup>1</sup> has stated that cure monitoring of thick samples is one area in which progress needs to be made. Hardness measurement is commonly used for cure monitoring in thick dental composites<sup>3</sup>. However, since hardness measurements can be made only during the final stages of cure when the resin is solid, it cannot be used for on-line cure monitoring. Photo dynamic mechanical analysis was recently used by Renault *et al*<sup>4,5</sup> for *in situ* monitoring of cure of neat or fiber filled resins. While this technique shows considerable promise it also has several limitations. It is based on the bulk tensile modulus of the entire sample rather than the cure behavior of the sample at a particular depth and requires the modulus of the resin to be correlated with the extent of cure. For these reasons it is not very useful for determining cure time of thick polymer samples.

In this study, the polymerization was monitored by measuring the temperature at the bottom of the sample during photopolymerizations carried out under adiabatic conditions. This method is based upon the fact that the polymerization process is highly exothermic, and, under adiabatic conditions, leads to a considerable temperature rise. Therefore, cure at the bottom of a thick sample can then be monitored by placing a

thermocouple on the bottom surface of the container. After the sample is illuminated, the observed temperature rises due to the heat of polymerization, and finally plateaus at a constant value when the polymerization is complete. The time at which the temperature becomes constant can be regarded as the cure time for that sample. Using this cure monitoring technique, the effect of several variables such as photoinitiator type, photoinitiator concentration, light intensity and spectral distribution, sample thickness *etc.* were studied and recommendations were made for design of initiating systems for photopolymerization of composites.

## 5.2. Experimental

### *Materials*

In these studies, Derakane 510A obtained from Dow Chemicals was used as the resin. The photoinitiators used included 2,4,6 Trimethyldiphenylbenzoyl phosphine oxide (TPO, BASF), bis(2,4,6-trimethylbenzoyl) phenylphosphine oxide (BAPO, Ciba-Giegy), benzoin ethyl ether (BEE, Aldrich) and bis[ $\eta^5$ -2,4-Cyclopentadien-1-yl] bis[2,6-difluoro-3-[1H-Pyrrol-1-yl]phenyl Titanium (a substituted titanocene, Ciba-Giegy). In addition a two component initiating system consisting of N-methyldiethanolamine (Aldrich) and camphorquinone (Aldrich) was investigated. Finally, in some systems benzoyl peroxide (Aldrich) was used as a thermal initiator. The fiber reinforcement used in the composites was an e-glass woven mat. All the chemicals were used as received.

### *Determination of Cure Time*

The formulation to be photopolymerized (which consisted of the resin and the photoinitiating system) was injected into a cylindrical polyethylene vial to the required thickness (thicknesses ranging from 9 mm to 29 mm were studied). A thermocouple (Chromium-Aluminium, Omega type K) was introduced through a small hole in the side of the vial. The thermocouple was positioned at the bottom of the sample, near the wall of the vial. Care was taken to ensure that the thermocouple was placed at the same position for every run. The thermocouple was connected to a WS-ABC interface card (Omega Inc.) which digitized the data and stored it in a PC. The vial was thermally insulated by a thick layer (several inches) of polyurethane foam in order to ensure that the polymerization was adiabatic. The sample was irradiated with light from above using a 1000 W Oriel model 66021 medium pressure mercury-xenon arc lamp which was equipped with a water filter to eliminate the IR radiation and a dichroic mirror to filter out the deep UV radiation (below 280nm) emitted by the lamp. Light intensity was measured using UVICURE Plus high energy UV integrating radiometer (EIT Inc.). In order to start the data collection and sample illumination simultaneously, a shutter (Oriel model 71445 electronic safety shutter) was triggered by a digital pulse from the WB-ASC interface card. The sample was illuminated for a predetermined period of time, and the acquired temperature-time data was analyzed to determine the cure time for the sample. Figure 5.1 shows the general trend followed by the temperature-time curve during such photopolymerizations. The time when the curve begins to plateau was taken to be the cure time for the specimen (200 seconds for the curve in figure 5.1). Three runs were

performed for each sample, and the variation in cure time was less than 5%.

### *Composite Preparation and Testing*

The UV cured composite specimens were prepared as follows: woven glass fiber mats were cut to the required dimensions, and were stacked on top of one another before the UV curable formulation was poured onto the stack. The resin-impregnated fiber mats were placed between two glass plates and pressure was applied to compress the uncured composite. The system was then exposed to light of 250 mW/cm<sup>2</sup> UVA intensity from a 3000 W arcless mercury vapor lamp (Fusion UV Systems, model F450T) for five minutes. The cured composite was then cut to the dimensions required for the flexural test. A similar procedure was followed for the thermally cured composite except that it was thermally cured in an oven at 75°C for 1 hour and postcured at the same temperature for 24 hours. The flexural properties of cured composite specimens were determined using a United STM-20 instrument in accordance with the ASTM D790 method. The composite specimens prepared for testing were 6 to 7 mm thick, 10 mm wide and 125 mm long. The span length used was 96 mm and the crosshead downdrive rate was 2.6 mm/min, as specified by the ASTM test procedure.

### *Absorption and Transmittance Spectra*

Transmittance spectra of the resins and absorption spectra of the photoinitiators used in this study were determined using a Hewlett Packard 8452A diode array UV-Vis spectrophotometer.

### *Emission Spectrum of Lamp*

Emission spectra of the lamp was obtained using a fiber optic spectrometer model SD1000 from Ocean Optics Inc.

## **5.3. Results and Discussion**

### *Spectral Considerations for the Choice of photoinitiator*

A number of commercially available photoinitiators may be used for photopolymerizations of films and coatings. However, for photocuring of thick parts, the criteria for selection of photoinitiator are more stringent. Foremost, the photoinitiator obviously must have significant absorbance in the region where the lamp emits. In addition, for thick parts, the photoinitiator must have good absorbance in a spectral region different from where the other components of the system (resin, additives etc.) absorb. This is because the resin constitutes more than 99% of the formulation and may effectively filter out the light which is required for photoinitiation. Finally, it is best if the photoinitiator undergoes significant bleaching upon illumination. This allows light penetration into the sample upon production of active centers.

Figure 5.2 shows the transmittance spectrum of the Derakane 510A resin in the 300-550 nm range. The figure illustrates that the resin is opaque to light of wavelength between 300 and 350 nm and the transmittance increases continuously at higher wavelengths. Figure 5.3 is a plot of the extinction coefficient of Derakane 510A, which

again reveals that the absorbance is very high below 350 nm and decreases rapidly at higher wavelengths. It is noteworthy that the extinction coefficient of the resin appears to be low (for example the extinction coefficient of the resin at 365 nm is 1.8 ml/gm cm as compared almost 2000 ml/gm cm for BAPO at the same wavelength). However, even such a small resin extinction coefficient becomes very important because it constitutes more than 99 % of the photocurable formulation. The extinction coefficient of the resin being investigated (Derakane 510A) and its dependence on the wavelength in the 300-450 nm region is a very important optical characteristic especially for UV curing thick parts since it dictates how much of the initiating light will be absorbed by the resin itself (and hence will not be available for photoinitiation). For example, attempts to photocure the resin using 330 nm light will fail since the resin is opaque at this wavelength, hence no photons will be available to the initiator to produce active centers which are required to initiate the polymerization.

Figure 5.4 compares the transmittance spectra of three different resins: a vinyl ester (Derakane 510A), a multifunctional acrylate (ditrimethylolpropane tetracrylate, DTMPTA,) and an epoxy resin (DER 362 from DOW), illustrating that the optical characteristics of different resins in the 300-500 nm region are significantly different. The DER 362 and the DTMPTA are more transparent in this spectral region and therefore are easier to photopolymerize using UV light.

Figure 5.5 shows the emission spectrum of a medium pressure mercury lamp commonly used for UV curing. It has prominent emission lines at 300, 312, 330, 365, 410 and 440 nm. Figure 5.6 shows the emission spectrum of light from the same lamp

after it is transmitted through Derakane 510A. It is clear that the resin completely absorbs the emission lines at 300,312 and 330 nm, however, it transmits the 365, 410 and 440 nm lines and the transmittance increases at higher wavelengths. These results are in concordance with the transmittance spectrum of the resin which was discussed earlier and serve to reinforce the point that the transmittance spectrum of the resin being cured is very important for photocuring of thick polymers.

The above results directly affect the choice of photoinitiator or photoinitiating system which can be used for photopolymerization of Derakane 510A. Obviously, the photoinitiating system must have significant absorbance in the 360-450 nm region in order to utilize the 365, 410 and 440 nm lines which are emitted by the lamp and transmitted by the resin. Several classes of commonly used photoinitiators such as benzoin ethers, dialkoxyacetophenones, hydroxy alkyl ketones, morpholino ketones, amino ketones *etc* do not meet this requirement. However, one class of photoinitiators, namely benzoyl phosphine oxides exhibit considerable absorbance above 360 nm. For example, Figures 5.7, 5.8 and 5.9 show the absorbance spectra of benzoin ethyl ether, trimethyldiphenylbenzoyl phosphine oxide (TPO) and bis(2,4,6 trimethylbenzoyl) phenyl phosphine oxide (BAPO). It is clear that TPO and BAPO have significant absorbance at 365 and 410 nm and are therefore good candidates for UV polymerization of Derakane 510A. Another significant motivation for selecting the benzoyl phosphine oxides is their tendency to photobleach efficiently in the UVA spectral region (as shown in Chapter 4).

*Effect of Photoinitiator Concentration on Cure Time*

Thermocouple studies performed on neat resin (Derakane 510A) revealed that for a given sample thickness and light intensity, there exists an optimum concentration of photoinitiator at which the cure time is a minimum. At initiator concentrations below the optimum, the cure time decreases with increasing initiator concentration as expected from simple kinetic considerations. At concentrations higher than the optimum the cure time actually increases with increasing concentration due to the optical density of the photoinitiator, which prevents light from penetrating into the sample. Figures 5.10, 5.11 and 5.12 show the effect of photoinitiator concentration on the cure time of neat resin (Derakane 510A) for TPO, BAPO and BEE respectively. In every case, it is seen that there exists an optimum initiator concentration at which the cure time is minimum. However, there is considerable difference in the optimum concentration and optimum cure times for the different photoinitiators. Table 5.1 summarizes the optimum cure times and concentrations for these three photoinitiators. Clearly, BEE exhibits a much higher cure time as compared to the phosphine oxide photoinitiators, a result which is consistent with the conclusions which were drawn based upon spectral considerations. Table 5.1 also reveals that the BAPO photoinitiator exhibits a lower cure time and a lower optimum concentration as compared to the TPO. Both these results can be explained based upon the photochemistry of the two initiators. Figure 5.13 shows that two radicals formed upon photolysis of a single TPO molecule. In comparison, Figure 5.14 illustrates that complete photolysis of BAPO results in more than two free radicals. The higher radical yield translates into high curing efficiency and consequently results in lower optimum

initiator concentration and lower cure time for the BAPO. A second factor contributing to this is the higher extinction coefficient of BAPO compared to TPO in the 360-420 nm region (as shown in Figure 5.15).

**Table 5.1.** Optimum concentration and cure times for three different photoinitiators for curing 0.9 cm thick sample of Derakane 510A with a light intensity of 65 mW/cm<sup>2</sup> UVA

Photoinitiator	Optimum Cure Time (sec)	Optimum Concentration (wt.%)
BAPO	160	0.2
TPO	220	0.4
BEE	620	0.3

#### *Effect of Photoinitiator Concentration on Degree of Conversion*

It was observed that the final temperature attained during the photopolymerizations was maximum at the optimum initiator concentration. This is shown in Figures 5.16 and 5.17 for two different photoinitiators (BAPO and TPO). Since all the experiments were carried out under adiabatic conditions, a higher temperature can only mean that more heat was released during the polymerization, implying that more double bonds were broken. This suggests that not only is the cure time a minimum at the optimum concentration but also the degree of conversion is maximum. This is in concordance with the result obtained by Guthrie *et al*<sup>6</sup> who concluded that the extent of polymerization (degree of conversion) of thick films (up to 5 mm) of multifunctional

acrylate and methacrylate reaches a maximum and then decreases with increasing concentration of photoinitiator.

These results illustrate that once a choice of photoinitiator has been made based upon spectral considerations, it is important to carry out further investigations to ascertain the optimum concentration of the initiator that is suitable for photocuring the sample of the required thickness. This is because use of the optimum photoinitiator concentration not only results in minimum cure time but also leads to maximum conversion. From these results it was concluded that use of 0.2 wt % BAPO was best for UV curing of 9 mm thick samples of Derakane 510A.

#### *Effect of Intensity on Cure Time*

Figure 5.18 illustrates the effect of light intensity on cure time for 9 mm thick Derakane 510A resin samples cured using the BAPO photoinitiator. Thus it is seen that increasing the intensity from 10 mW/cm<sup>2</sup> to 20 mW/cm<sup>2</sup> resulted in a dramatic decrease in the cure time from 480 to 240 seconds. However, further increase in intensity did not change the cure time as rapidly. This diminishing effect of increased light intensity is probably due to saturation of the excited singlet state of the photoinitiator. When the system is saturated, the rate of production of active centers is governed entirely by the rate of  $\alpha$ -cleavage, rather than by the rate at which the excited states are produced. Thus, above an intensity of 30 mW/cm<sup>2</sup>, increasing the light intensity leads to little change in the rate of production of active centers, and the cure time decreases only slightly.

### *Effect of Sample Thickness on Optimum Concentration*

Experiments performed on photocuring of thick polymer parts using BAPO photoinitiator showed a small decrease in optimum initiator concentration with increase in sample thickness (Table 5.2). This decrease in optimum initiator concentration enables more light to penetrate the sample to compensate for the decrease in light intensity that reaches the bottom of the sample with increased sample thickness.

**Table 5.2.** Effect of sample thickness on optimum concentration of BAPO

Thickness of Cured Resin (cm)	Optimum Concentration of BAPO (wt. %)
0.9	0.20
2.2	0.16
2.9	0.14

### *Hybrid Photoinitiator Systems*

As mentioned earlier, one of the considerations for the choice of a photoinitiating system is its ability to utilize all the light emitted by lamp. The lamp used in this study emits three lines 365, 410 and 440 nm where the resin transmits. As shown before, the photoinitiator BAPO absorbs the 365 and 410 nm lines. However, the 440 nm line is not absorbed (as shown in Figure 5.19) and hence is not used for production of active centers. Attempts were made to further reduce the cure time by utilizing the 440 nm line by means of a hybrid photoinitiating system. Essentially, this involves use of a photoinitiating

system consisting of BAPO plus a second photoinitiator which absorbs at 440 nm. Figures 5.20 and 5.21 show the absorption spectra of two photoinitiators (a substituted titanocene and camphorquinone) which were studied. Both these initiators have good absorbance at 440 nm. The formulation containing the hybrid photoinitiator system BAPO+titanocene actually showed a small increase in cure time over the formulation containing BAPO alone. This is probably because the titanocene has good absorbance at 365 and 410 nm in addition to 440 nm. This results in the light emitted at these wavelengths also to be absorbed by the titanocene rather than by the BAPO. Since the titanocene does not have good initiation efficiency (due to its bulky structure), it resulted in an increase rather than in a decrease in cure time. The camphorquinone+amine+BAPO formulation also did not show any significant decrease in cure time. This is probably because camphorquinone produces active centers by a diffusion controlled reaction with the amine and this reaction is too slow compared to the rapid  $\alpha$ -cleavage reaction of the BAPO to have any significant effect on the cure time.

#### *Dual Photo/Thermal Cure Systems*

Coons *et al*<sup>8</sup>, prepared vinyl ester/glass fiber composites by photopolymerization using BEE as the photoinitiator. They showed that addition of a thermal initiator (benzoyl peroxide) in addition to the photoinitiator resulted in a considerable decrease in cure time. This was explained based on the fact that the heat released during the photopolymerization process triggers the thermal initiator thereby resulting in the production of more active centers and hence faster cure. However, experiments

performed with the dual cure systems using BAPO as the photoinitiator and BPO as the thermal initiator revealed no significant reduction in cure time as compared to systems containing only BAPO. Coons et al<sup>8</sup> found that the cure time of 9 mm thick samples decreased from 900 seconds to about 300 seconds upon addition of 0.2 wt % of benzoyl peroxide along with 0.1 wt % of benzoin ethyl ether and further increase in the benzoyl peroxide concentration did not result in further reduction of the cure time. The cure time of 9 mm thick samples cured using 0.2 wt % BAPO alone was shown to be about 160 seconds, faster than the cure time of dual cured (BEE + BPO) samples. This shows that the production of active centers by the thermal initiator was not rapid enough to affect the polymerization rate of samples cured using BAPO alone.

#### *Composite Preparation & Testing Studies*

Glass fiber reinforced composites, 6 mm thick, containing 50 wt.% e-glass woven mat as the reinforcement and Derakane 510A as the matrix were prepared and their mechanical properties were determined. Three types of composites were prepared – (i) Purely photocured composite which contained 0.2 wt.% BAPO as the initiator (0.2 wt. % was used since it has earlier been established as the optimum for 9mm thick samples and the optimum concentration does not change significantly with thickness) (ii) Dual photo/thermal cured composite which contained 0.2 wt.% BAPO and 0.5 wt.% BPO as the initiating system (iii) Thermally cured composite containing 1.2 wt.% BPO as the initiator.

Figure 5.22 compares the flexural properties of the composites prepared. It is

clearly seen that there is no significant difference in the properties of the composites. It is important to note that the thermally cured composite was prepared by baking in an oven for 1 hour at 75°C to achieve complete cure and subsequently postcuring at the same temperature for 24 hours and it required 1.2 wt.% BPO, whereas the UV cured composite was cured only for 5 minutes at 250 mW/cm<sup>2</sup> UVA intensity using only 0.2 wt.% of the BAPO photoinitiator. This clearly demonstrates that UV curing leads to considerably faster cycle times as compared to thermal curing and results in a composite with the same mechanical properties as the traditional thermally cured composite. Using a thermal initiator along with the photoinitiator does not have any effect on the mechanical properties and it was earlier shown that it does not have a significant effect on the cure time either. Hence, there is no advantage in using the dual cure scheme with the BAPO photoinitiator.

#### **5.4. Conclusions**

In this contribution, it has been established that of all the photoinitiators studied, Bis(2,4,6-trimethylbenzoyl) phenyl phosphine oxide (BAPO) resulted in minimum cure time for the photopolymerization of thick samples of Derakane 510A using the mercury vapor lamp as the light source. It was also shown that there exists an optimum concentration of photoinitiator at which the cure time is a minimum. This optimum decreased slightly with increase in sample thickness. Studies conducted using hybrid and dual cure initiating systems with BAPO as one of the initiators revealed that there was no significant advantage of utilizing these schemes. Finally, it was shown that the flexural

properties of glass fiber reinforced composites prepared by UV curing was comparable to those prepared by traditional thermal curing. More importantly, the time required for preparation of the composite by UV curing was considerably lower than the time required for preparation by thermal curing. This suggests that cycle times for preparation of glass fiber reinforced composites can be significantly reduced by using UV rather than thermal curing techniques.

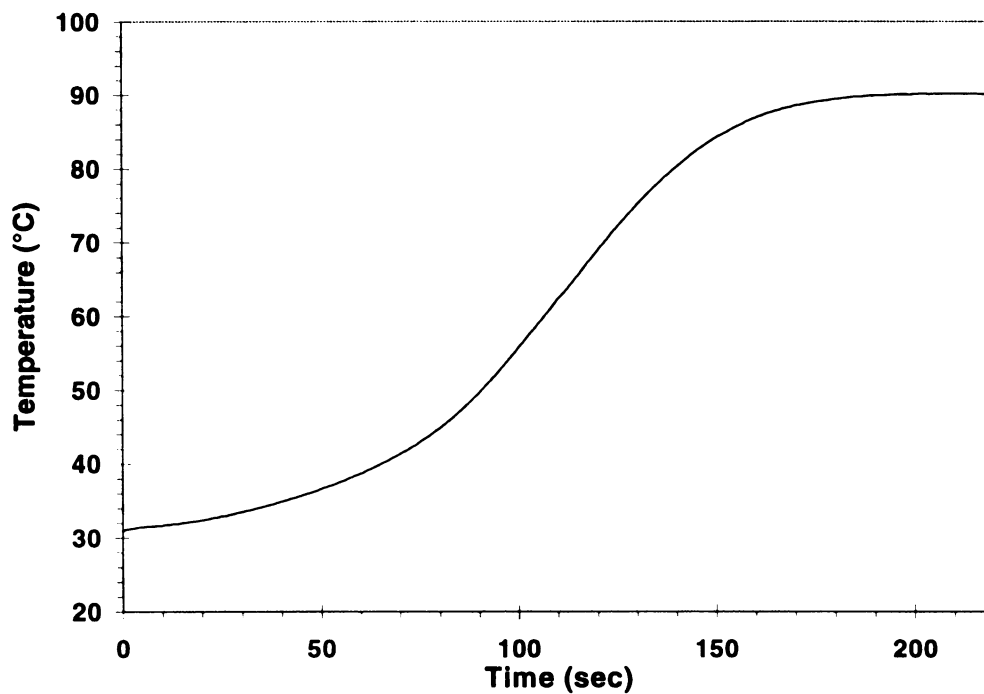


**Figure 5.1.** Variation of temperature as a function of time at the bottom of thick samples which are photopolymerized under adiabatic conditions

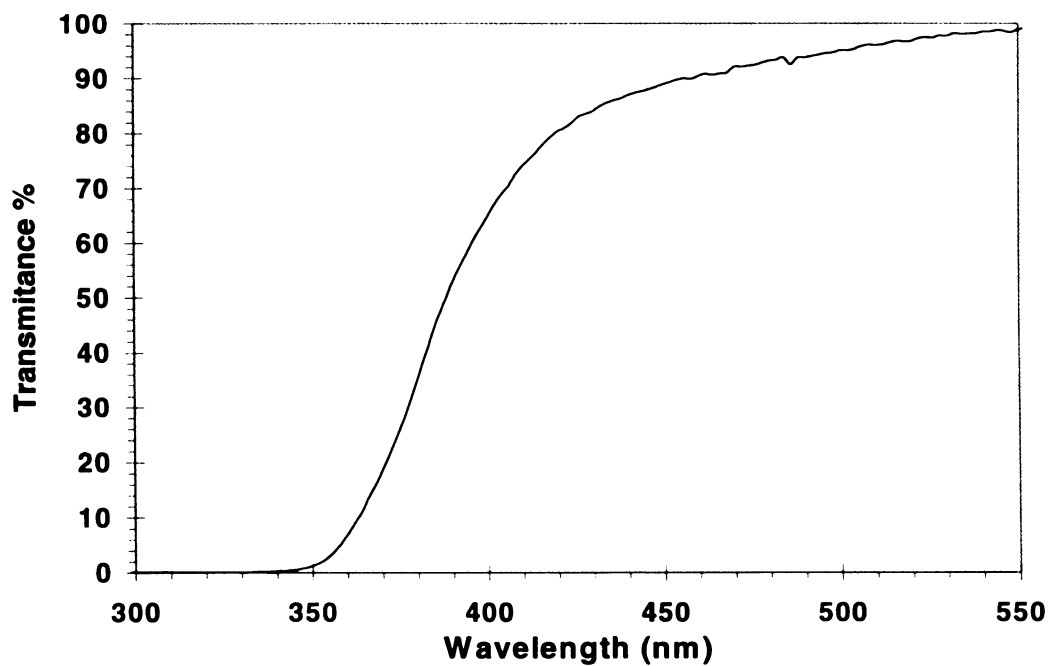


**Figure 5.2.** Transmittance spectrum of Derakane 510A in the 300-500 nm range. The path length used was 1 cm

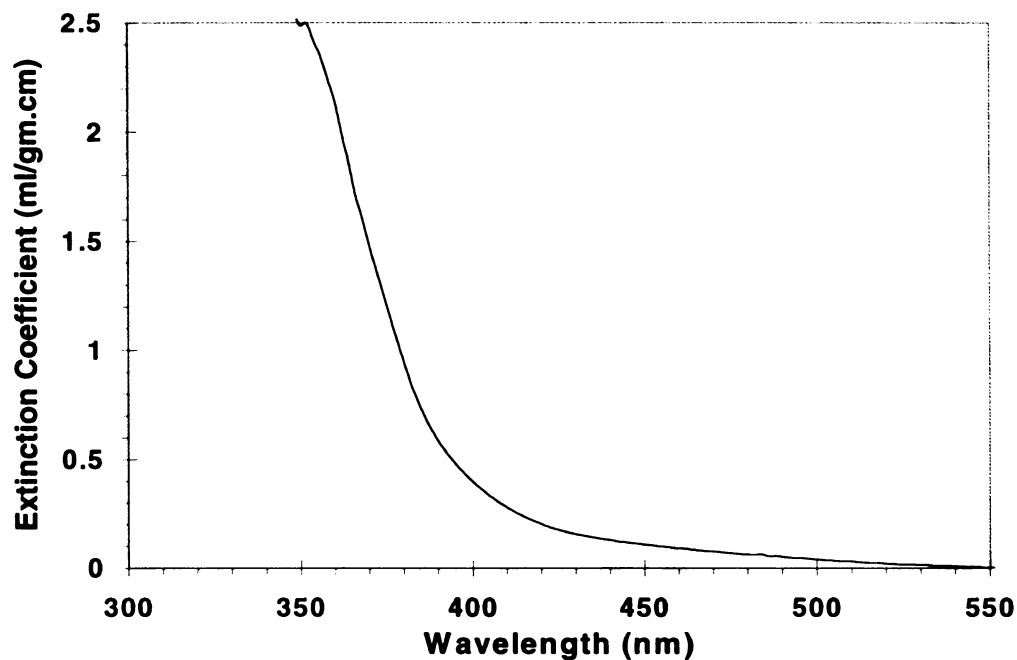


**Figure 5.3.** Plot of the extinction coefficient of Derakane 510A as a function of wavelength in the 350-550 nm range. The density of the resin is 1.2 gm/ml.

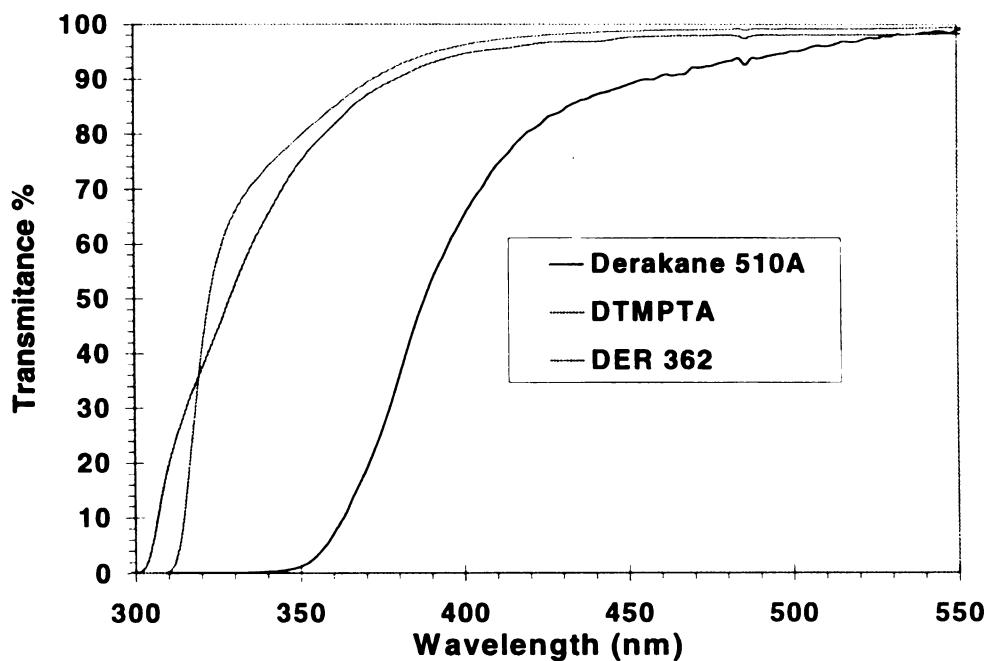


**Figure 5.4.** Comparison of the transmittance spectra of three different resins in the 300-550 nm range. The path length used was 1 cm in all cases.

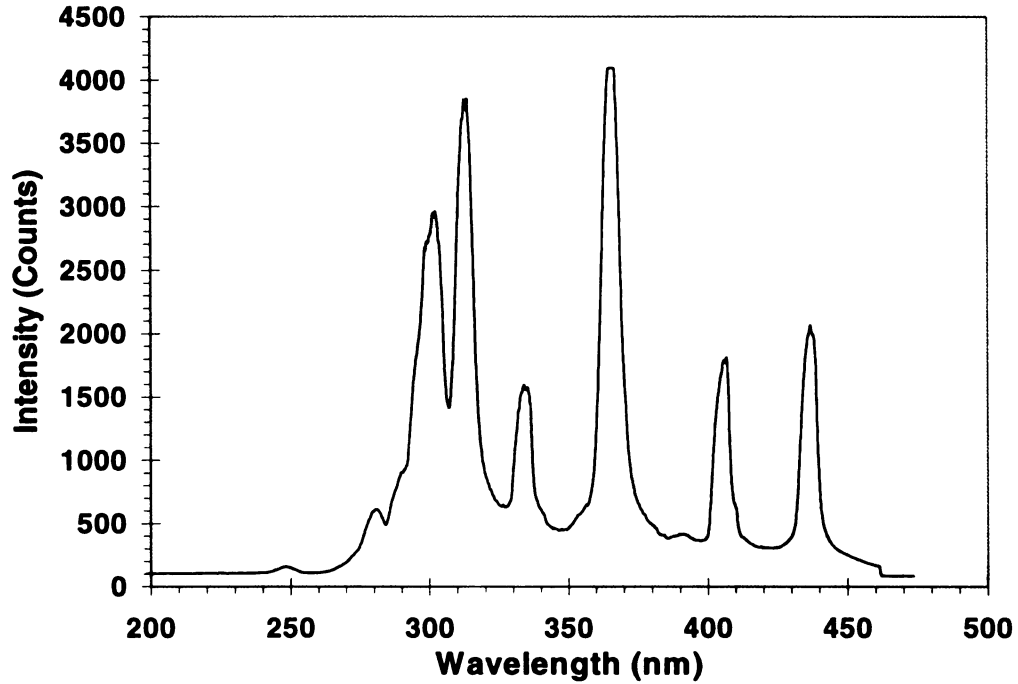


**Figure 5.5.** Emission Spectrum of the 1000 W Hg vapor lamp in the 280-500 nm region

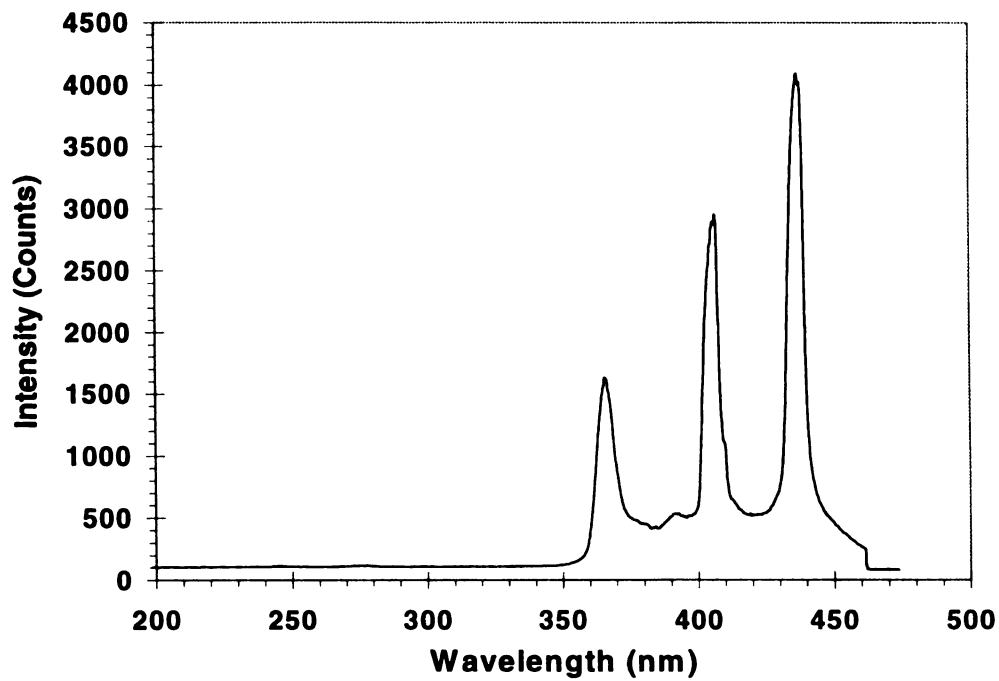


**Figure 5.6.** Emission spectrum of 1000 W Hg vapor lamp in the 280-500 nm region after it is transmitted through 0.9cm thick layer of Derakane 510A resin.

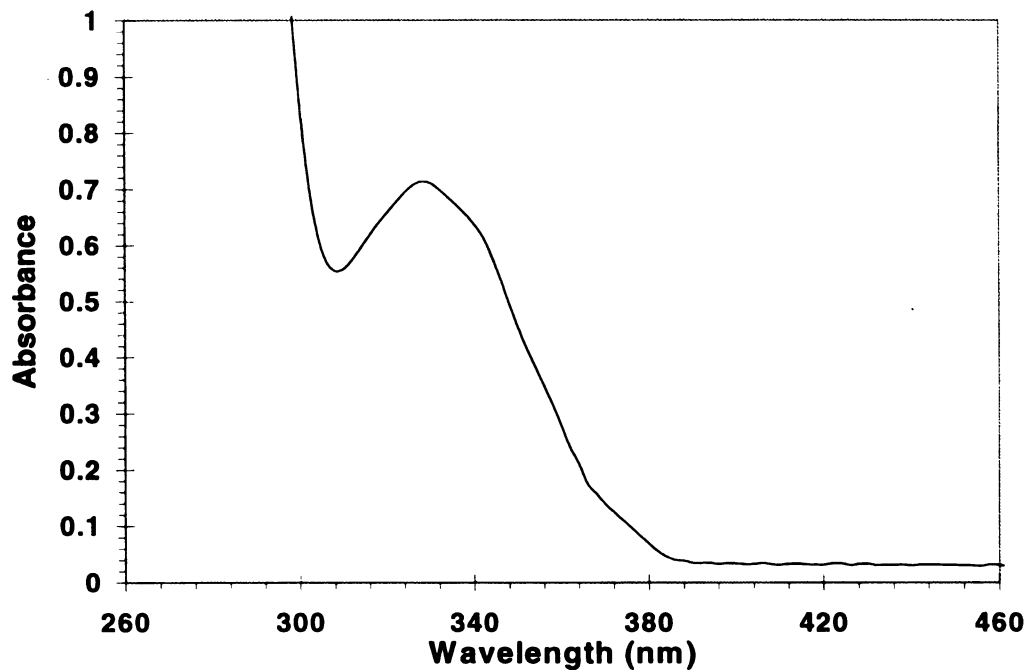


**Figure 5.7.** Absorption spectrum of Benzoin Ethyl Ether. The concentration is  $5.1 \times 10^{-4}$  g/ml in acetone

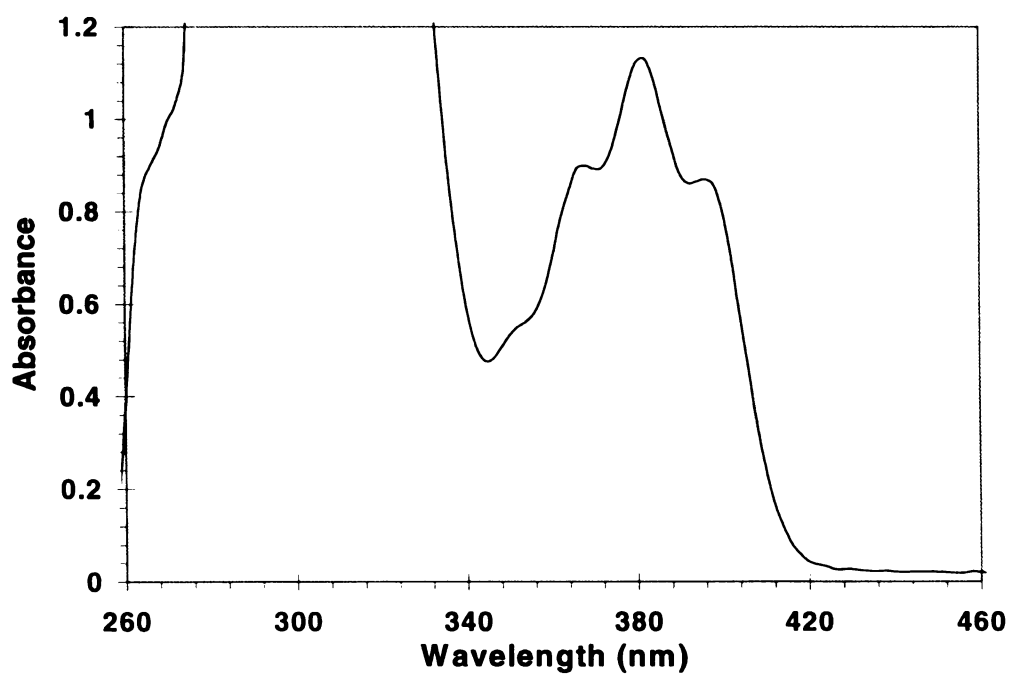


**Figure 5.8.** Absorbtion spectrum of TPO. The concentration is  $6.4 \times 10^{-4}$  g/ml in 2-propanol

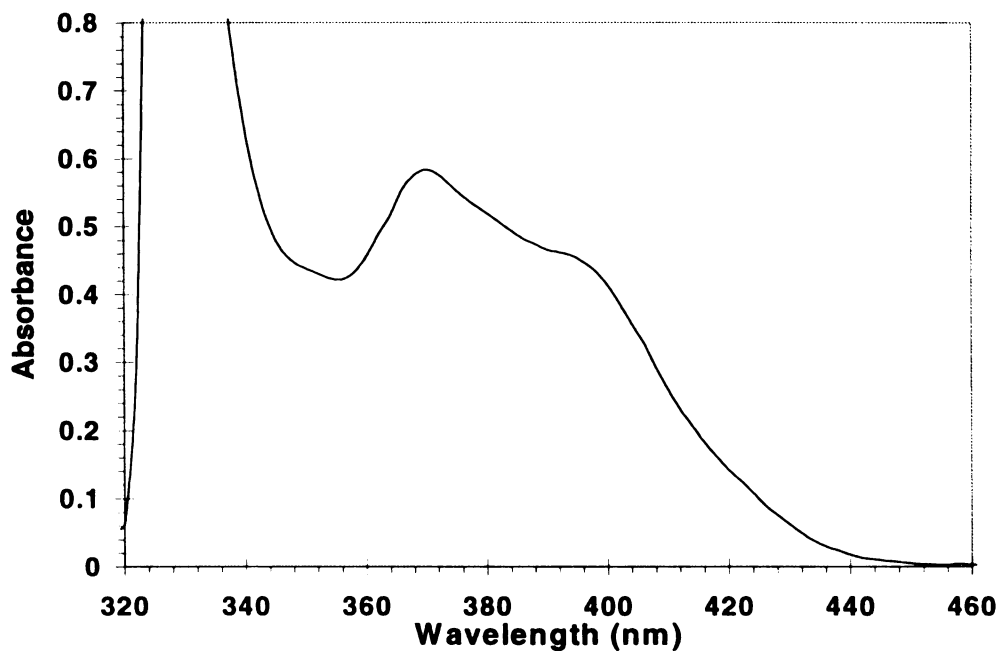


**Figure 5.9.** Absorption spectrum of BAPO. The concentration is  $5.1 \times 10^{-4}$  g/ml in acetone

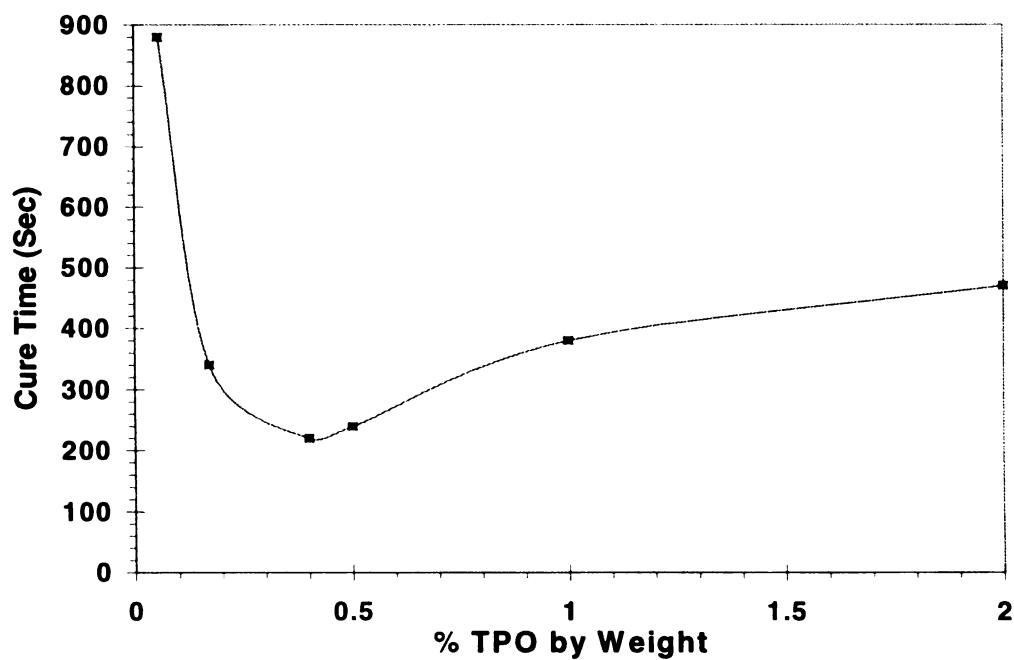


**Figure 5.10.** Optimum concentration of TPO for curing 0.9 cm thick sample of Derakane 510A. The light intensity used was  $65 \text{ mW/cm}^2$  UVA.

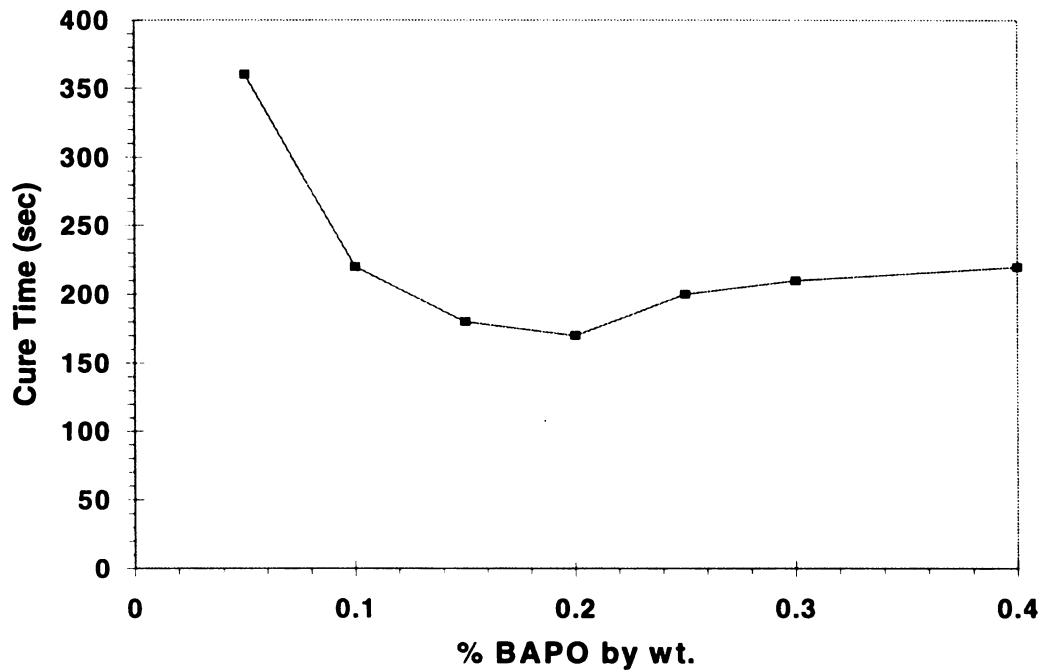


**Figure 5.11.** Optimum concentration of BAPO for curing 0.9 cm thick sample of Derakane 510A. The light intensity used was  $65 \text{ mW/cm}^2$  UVA.

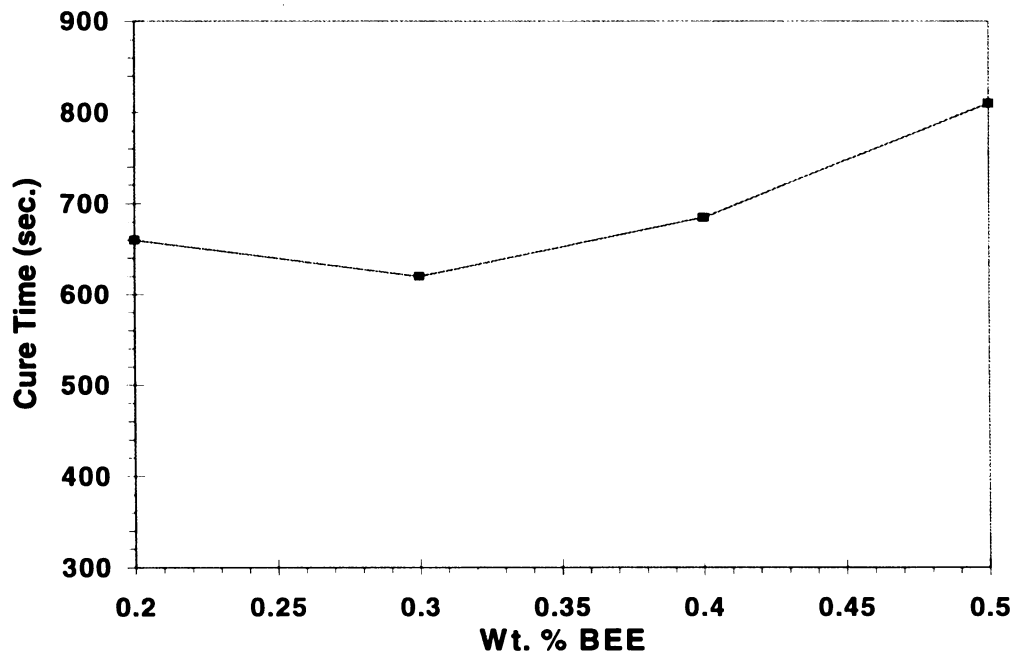


**Figure 5.12.** Optimum concentration of BEE for curing 0.9 cm thick sample of Derakane 510A. The light intensity used was  $65 \text{ mW/cm}^2$  UVA.

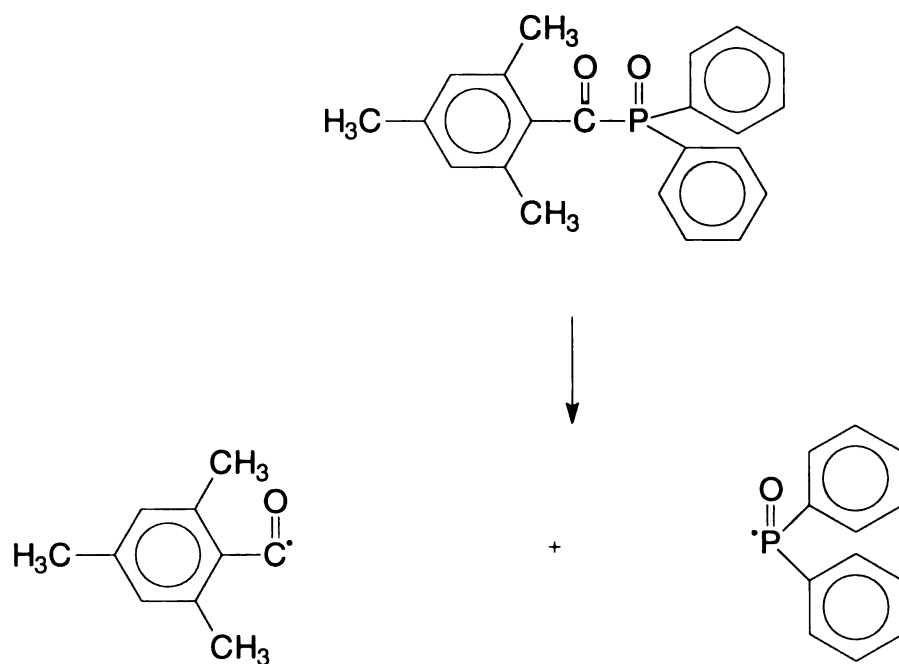


**Figure 5.13.** Radicals formed by photolysis of TPO

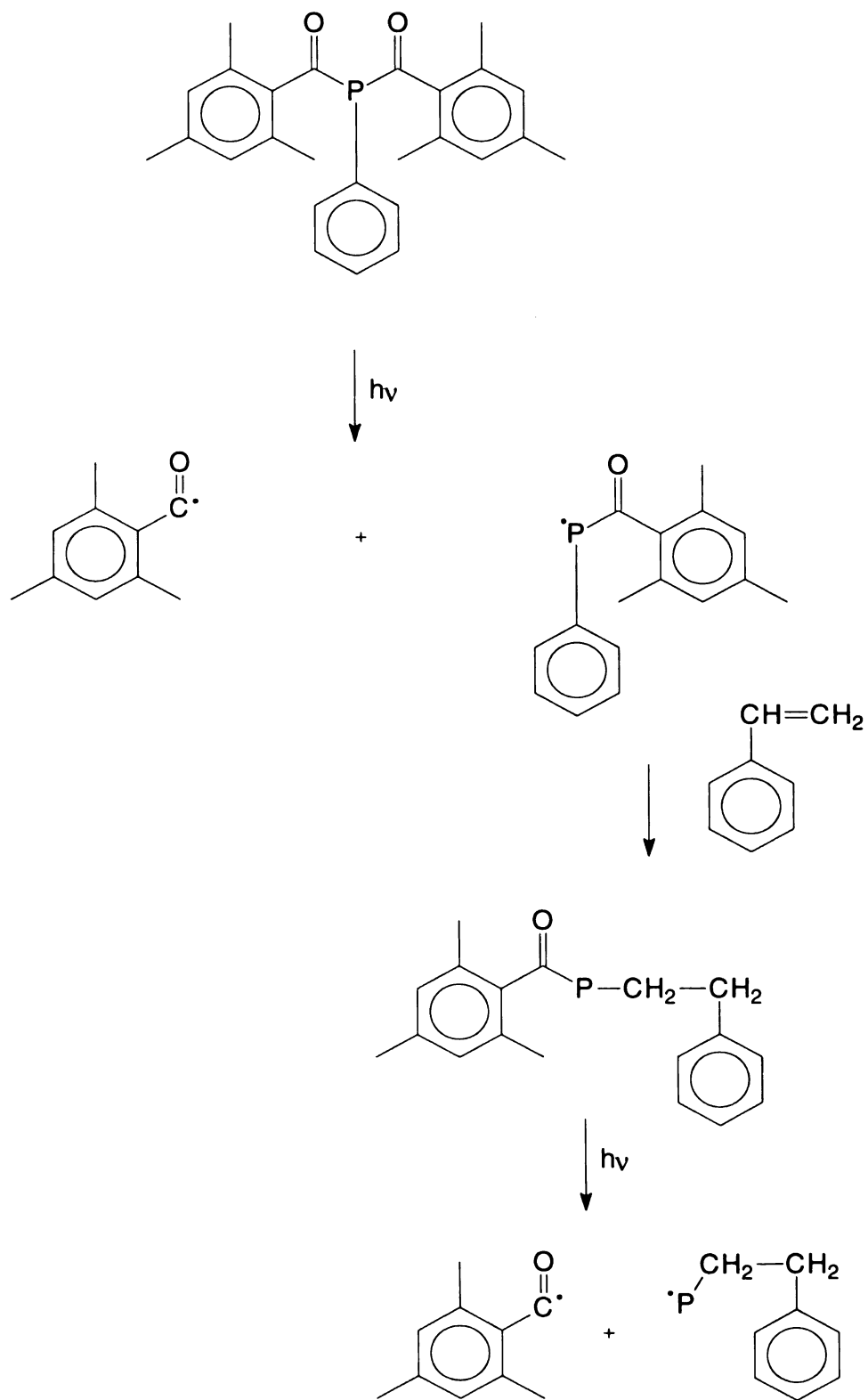


**Figure 5.14.** Radicals formed during complete photolysis of BAPO

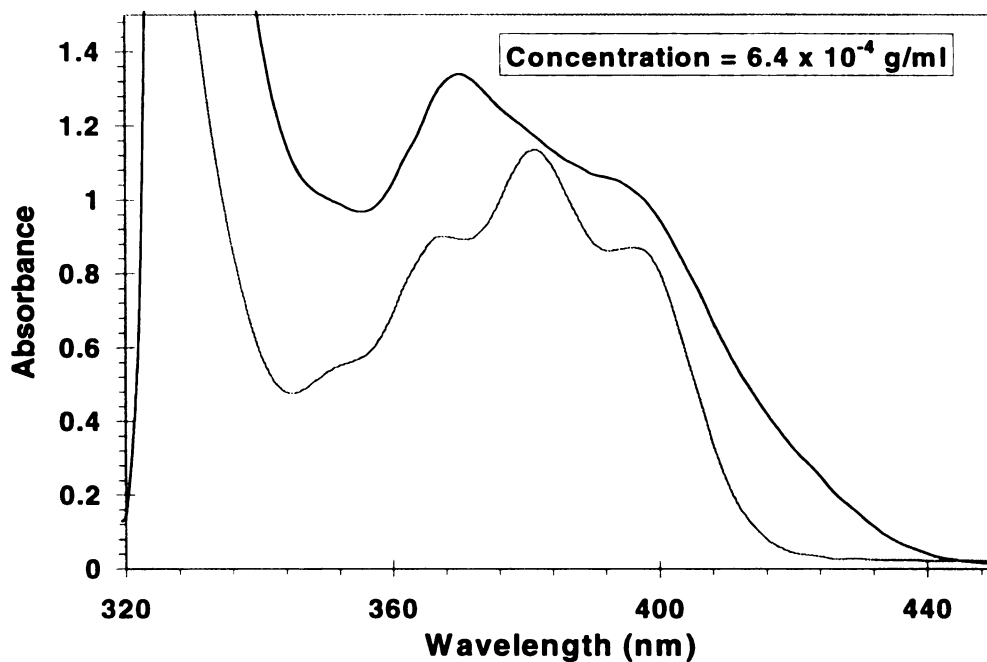


**Figure 5.15.** Comparison of the absorption spectra of TPO and BAPO in the 320-450 nm spectral region

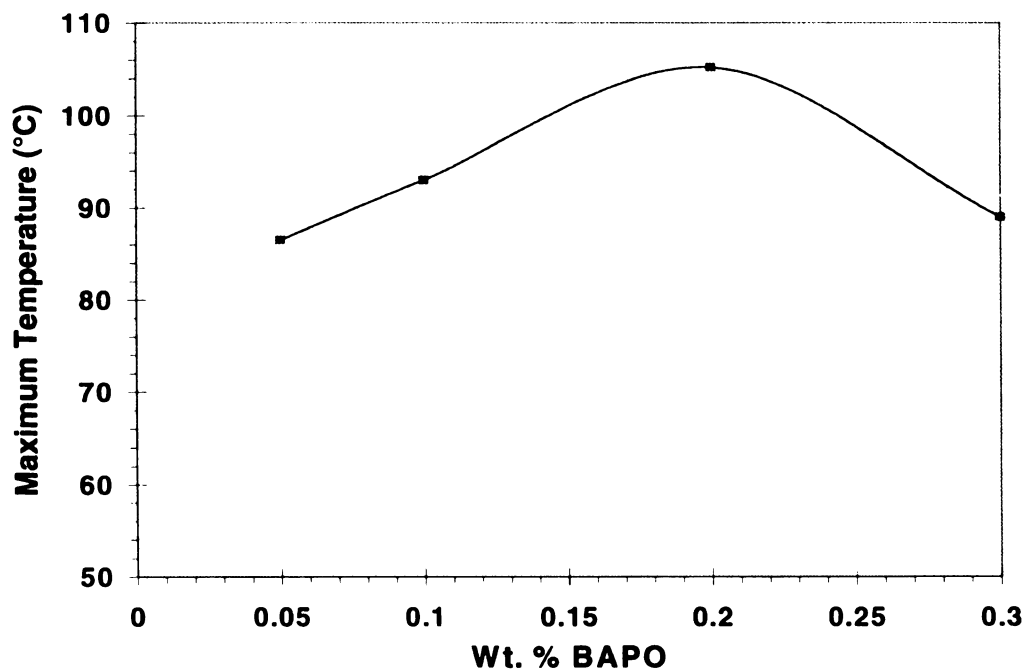


**Figure 5.16.** Maximum temperature measured by the thermocouple during BAPO initiated photopolymerizations of 0.9 cm thick samples of Derakane 510A. The light intensity used was  $65 \text{ mW/cm}^2$  UVA

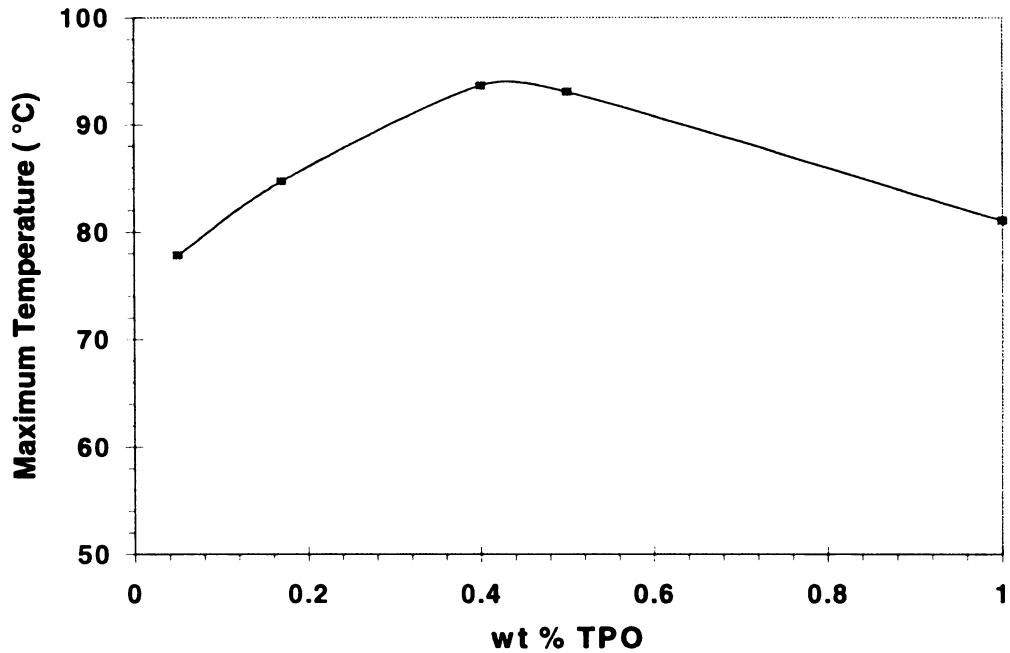


**Figure 5.17.** Maximum temperature measured by the thermocouple during TPO initiated photopolymerizations of 0.9 cm thick samples of Derakane 510A. The light intensity used was 65 mW/cm<sup>2</sup> UVA

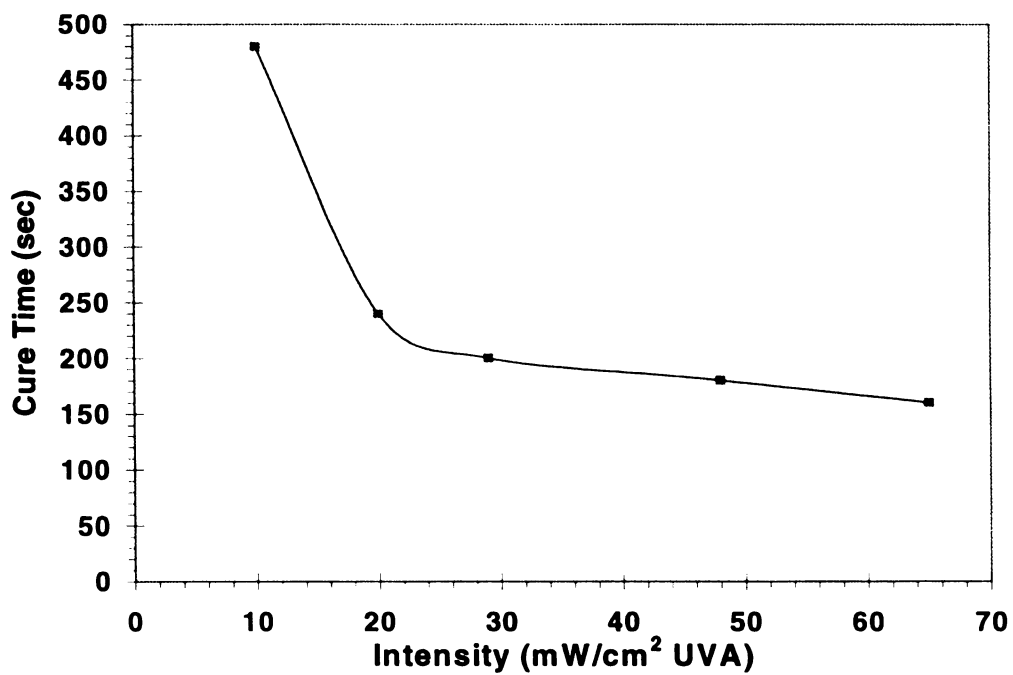


**Figure 5.18.** Effect of light intensity on cure time of 0.9 cm thick sample of Derakane 510A

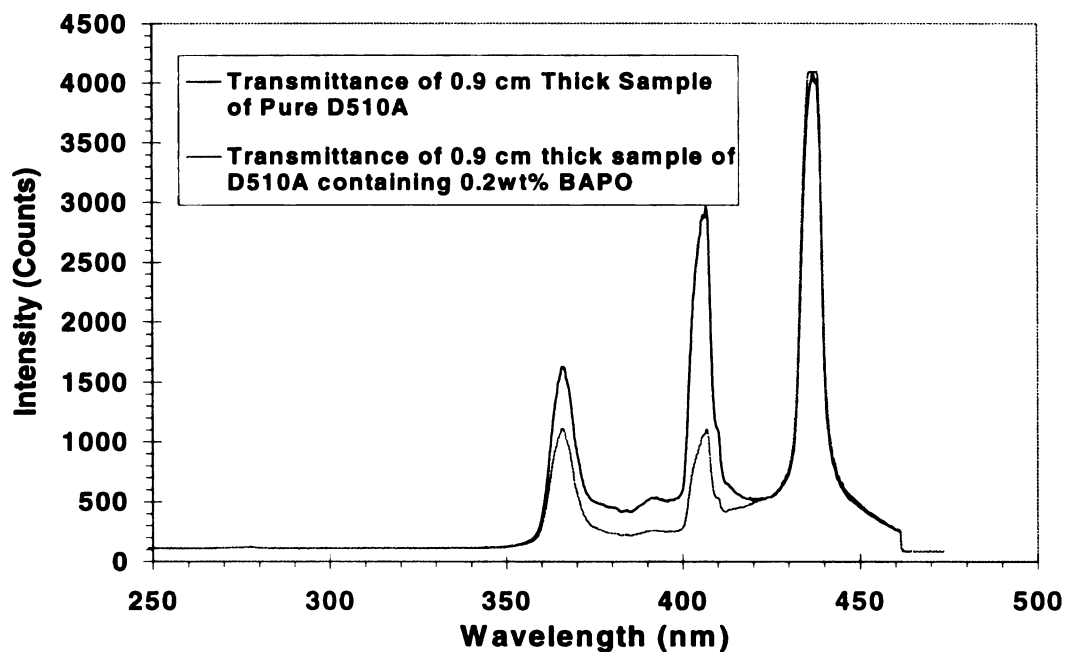


**Figure 5.19.** Comparison of emission spectra of Hg vapor lamp after passing through 0.9 cm thick sample of Derakane 510A resin with and without BAPO photoinitiator

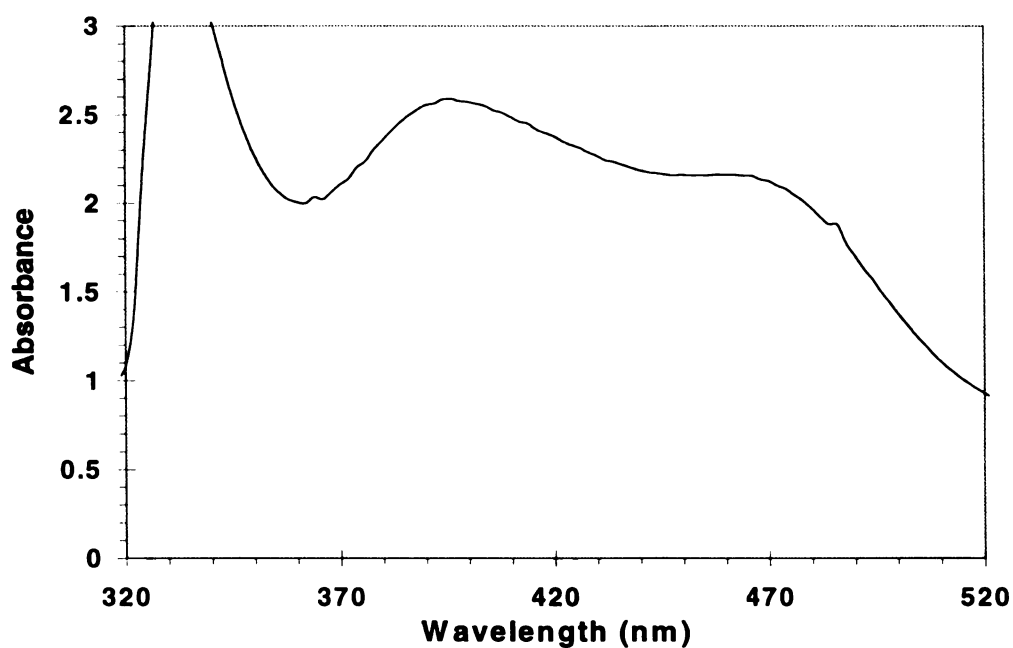


**Figure 5.20.** Absorbance spectrum of Bis [ $\eta^5$ -2,4-Cyclopentadien-1-yl] bis[2,6-difluoro-3-[1H-Pyrrol-1-yl] phenyl] titanium. The concentration is  $2.4 \times 10^{-3}$  g/ml in acetone

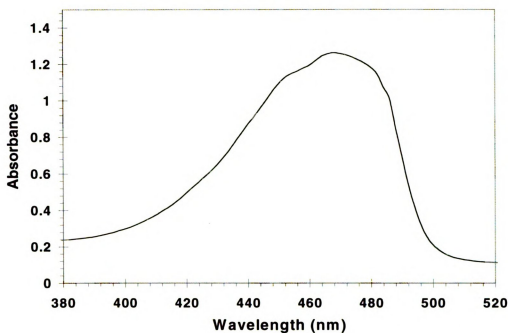


**Figure 5.21.** Absorption spectrum of Camphorquinone in the 380-520 nm region. The concentration is  $5.01 \times 10^{-3}$  g/ml in acetone

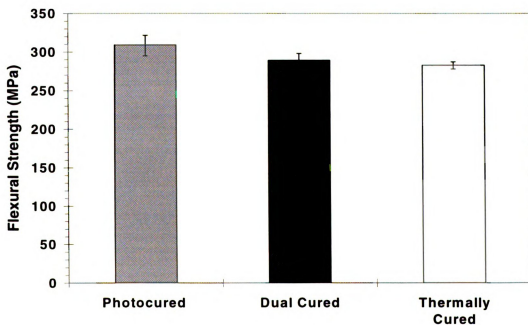


**Figure 5.22.** Comparison of flexural strength of composites. The bar represents the average value (of 5 samples) while the error bars represent the high and low values obtained in the tests

### 5.5. List of References

1. A.K. Davies, *Radiation Curing of Polymers II*, D.R. Randell ed., The Royal Society of chemistry, 1991
2. J.F. Rabek, *Radiation Curing in Polymer Science and Technology, Volume I*, J.P. Fouassier and J.F. Rabek eds., Elsevier, 1993
3. R. Tirtha, P.L. Fan, J.B. Dennison, J.M. Powers, *J Dent Res*, **61**, 1184, 1982
4. T. Renault and A.A. Ogale, *Polym Engg. Sci.*, **36**, 551, 1996
5. T. Renault, A.A. Ogale, M.J. Drews, *Proc. ANTEC '93*, 2352, 1993
6. J. Guthrie, M.B. Jaganathan, M. S. Otterburn, J. Woods, *Polymer Bulletin*, **15**, 51, 1986
7. K. Dietliker, G. Hug, R. Kaeser, M. Kohler, U. Kolczak, D. Leppard, L. Misev, G. Rist, W. Rutsch, *Novel High Performance Bisacylphosphine Oxide (BAPO) Photoinitiators*, Ciba-Geigy Corporation, 1994
8. Coons, L.S., Rangarajan, B., Godshall, D., and Scranton, A.B., *ACS Symposium Series*, in press

## Chapter 6

### Summary and Recommendations

#### 6.1 Summary

##### *Model for Photobleaching*

A fundamental mathematical model was developed to characterize the photobleaching of initiators when exposed to monochromatic light of the appropriate wavelength. Given the incident light intensity and wavelength and the initial photoinitiator concentration, the model predicts the variation of the photoinitiator concentration and light intensity with time and sample depth. The model was verified experimentally for four different  $\alpha$ -cleavable photoinitiators: benzoin ethyl ether, trimethyldiphenylbenzoylphosphine oxide, bis(2,4,6-trimethylbenzoyl) phenyl phosphine oxide and a substituted titanocene. The model proved to be very useful firstly because it quantified the photobleaching effect in terms of three constants which could easily be determined, and secondly because it helped in comparing the photobleaching effectiveness of different initiators and thereby in making a choice of photoinitiator for curing of thick polymer and composite parts. For example it was shown that the phenyl phosphine oxide initiator (BAPO) undergoes more efficient bleaching than benzoin ethyl ether.

*Investigation of Photoinitiating Systems for Photopolymerization of Composites*

Studies were performed to evaluate the suitability of different photoinitiators for photocuring of thick polymer and composite parts. The benzoyl phosphine oxide photoinitiators were chosen for further studies based upon their absorption spectra, the emission spectrum of the UV lamp used and transmittance of the resin. The photoinitiators chosen were then used to cure thick resin samples and the final choice of initiator was made based upon cure time considerations. Studies were performed to determine the effect of light intensity, photoinitiator concentration and sample thickness on the cure time of the resins. It was shown that there exists an optimum photoinitiator concentration at which the cure time is minimum and conversion is maximum. The results indicated that BAPO was the best photoinitiator and the optimum concentration was 0.2 wt.%. It was observed that increasing the light intensity reduced the cure time dramatically up to the point when saturation occurred and increasing the intensity beyond this point did not reduce the cure time as rapidly. Studies performed to evaluate the effect of sample thickness on cure time indicated that increasing the sample thickness resulted in a small decrease in the optimum photoinitiator concentration. Hybrid photoinitiating systems and dual photo/thermal cure schemes were investigated in an attempt to further reduce the cure time. Finally, composite samples were prepared both by photocuring and by thermal curing, their mechanical properties were evaluated and found to be equal.

## 6.2 Recommendations for Future Work

### *Choice of Photoinitiating System*

BAPO was found to be the best photoinitiator for the system under consideration. However, it was shown that the 440nm line emitted by the lamp was not utilized and attempts to utilize this line by adding initiators that absorbed in this region were not successful. This shows that behavior of hybrid photoinitiating systems is not so simple. Further studies need to be conducted to understand how hybrid photoinitiator systems work. Similar studies need to be conducted on dual photo/thermal initiating systems.

### *Development of a Polychromatic Photobleaching Model*

The model developed in this thesis is applicable only if the light source is monochromatic (or almost monochromatic). However, in several practical applications involving photobleaching, the light source emits at several different wavelengths. For example the commonly used mercury vapor lamp has at least 5 different emission lines in the UVA spectral region. Hence, another area for future work is extension of the monochromatic photobleaching model to polychromatic photobleaching.

### *Model for Photopolymerization of Thick Polymer Parts*

To arrive at a model for photopolymerization of thick polymer parts, it is necessary to combine the photobleaching model with a suitable model for the polymerization kinetics. Most of the models for polymerization kinetics are either too complicated or make the quasi steady state assumption which is incorrect. One possible

kinetic model that can be used is an empirical model proposed by Pusatcioglu et al<sup>1</sup>. The model incorporates empirical constants which must be determined from experiment. However, the model is being widely used to study polymerization kinetics either directly or with minor modifications<sup>2,3,4</sup>. Thus, one possible area for further study is the development of a working model for photopolymerization of thick polymer parts by combining the photobleaching model with the model for polymerization kinetics.

#### *Development of Cure Monitoring Techniques for Thick Systems*

There are very few techniques available for cure monitoring of thick systems. Development of more efficient and reliable methods for monitoring the cure of thick systems will undoubtedly lead to a better understanding of the photocuring process and will result in highly efficient photopolymerization techniques which could eventually completely replace thermal cure.

### **6.3. List of References**

1. S. Y. Pusatcioglu, A.L. Fricke, J. C. Hassler, *J. Appl. Polym. Sci.*, **24**, 937, 1979
2. J. M. Kenny, A. Maffezzoli, L. Nicolais, *Composites Science and Technology*, **38**, 339, 1990
3. M. R. Kamal, S. Sourour, M. Ryan, *Polym. Eng. Sci.*, **13**, 59, 1973
4. H. Han, K. W. Lem, *J. Appl. Polym. Sci.*, **28**, 3155, 1983